Renewable Energy 154 (2020) 581–597

Contents lists available at ScienceDirect

Renewable Energy

journal homepage: www.elsevier.com/locate/renene

Assessment of the Stirling engine performance comparing two renewable energy sources: Solar energy and biomass

Ana Cristina Ferreira [a, b, *], João Silva [a, b], Senhorinha Teixeira [a], José Carlos Teixeira [b], Silvia Azucena Nebra [c]

[a] ALGORITMI Research Centre, University of Minho, Guimarães, Portugal
[b] MEtRICs Research Centre, University of Minho, Guimarães, Portugal
[c] Engineering, Modelling & Applied Social Sciences Centre, Federal University of ABC, Brazil

ARTICLE INFO

Article history:
Received 30 November 2019
Received in revised form
13 February 2020
Accepted 7 March 2020
Available online 11 March 2020

Keywords:
Stirling engine
Renewable energy sources
Solar energy
Biomass burner
Energy efficiency

ABSTRACT

The paper addresses the assessment of the Stirling engine performance by comparing biomass and solar energy as external renewable energy sources. A program-code was developed in the MatLab® to solve the thermal model of an alpha-Stirling engine, accounting for the limitations in the heat transfer processes in the regenerator and the losses due to pumping effects. The solar energy source was modelled as a concentric solar dish collector, considering a receiver located at the focal point and designed to absorb the maximum possible of the solar radiation. Regarding the biomass system, the temperature of the flue gases leaving the bed is computed through an energy balance, considering the fuel energy introduced into the bed, the energy that is provided by the bed and the incident radiation in the bed. The simulation results show that the biomass-fuelled Stirling engine provided 87.5% more power output than the solar energy source, with an efficiency of 46.67%. Also, the average receiver temperature from the solar source is about 775 K, whereas, in the boiler bed, the temperature reaches the value of 1288 K. In the solar-dish modelling, the reflected radiation that passes into the cavity receiver depends on the aperture ratio and rim angle. It was proved that a rim angle of at least 45° is required to ensure lower focal distances. Otherwise, the Stirling receiver needs to be far from the surface of the dish, resulting in higher thermal losses and lower temperature inside the receiver cavity. In biomass-fuelled system, it was shown that the temperature of the flue gases increases with the increasing the radiation flux, and decreases for higher split percentages between the primary and secondary air. The study also revealed the need to investigate the combustion stability regarding the particle emission in the flue gas, which can reduce the temperature close to the hot cylinder of the Stirling engine. The LCoE for the solar-power system is of about 1658 €/kWh, which is 52% higher when compared with the biomass-fuelled system (0.109 €/kWh). In conclusion, biomass-fuelled Stirling engines are able to provide a higher power output with higher thermal efficiency, avoiding the problems usually related to solar energy intermittency.

1. Introduction

The limitation of the world's natural resources and the need for their valorisation has increased the demand for a change in energy conversion technologies. Such change would enhance energy safety; promote enduring economic growth and prevent negative environmental impacts. In this sense, several initiatives and policies have emerged to support energy production in a more sustainable way. The use of renewable sources and Combined Heat and Power (CHP) is considered a good alternative to achieve sustainability milestones: cleaner and more efficient energy production [1,2]. Energy conversion systems based on CHP principle has been developed to meet the energy needs for the building sector in urban areas. Technologies, such as Stirling engines promote the high-efficiency energy conversion, contributing to more proficient use of resources and higher potential to reduce overall costs [3]. Cogeneration technologies are suitable to achieve the energy targets since they allow high primary energy savings and substantial reductions in CO_2 emission, which represents a large contribution

* Corresponding author. ALGORITMI Research Centre, University of Minho, Guimarães, Portugal.
E-mail address: acferreira@dps.uminho.pt (A.C. Ferreira).

https://doi.org/10.1016/j.renene.2020.03.020
0960-1481/

in delivering the targets of the Kyoto Protocol on climate change in Europe [4].

Small and micro-scale systems are usually designed to provide electricity in the range of 1–50 kW_{el} and fairly larger heating loads to meet the building energy needs [5,6]. The Stirling engine is one of the technologies applied to micro-scale applications [7–9]. These engines rely on an external combustion or exterior heat-sources, whereas the working fluid (i.e. air, helium, nitrogen or hydrogen) operates on a closed regenerative thermodynamic cycle, with cyclic compression and expansion processes [10,11]. The pressure variation of the working fluid is the result of the repeated heating and cooling phenomena, causing the piston movement. The piston movement is converted into useful mechanical work, through a mechanically driven system [12,13]. The thermodynamic cycle of a Stirling engine is quite similar to *Carnot*, replacing two isothermal transformations by two isochoric processes. High theoretical efficiencies can be achieved considering the ideal conditions, but there is a thermal limit for the operational condition of the heater and cooler temperatures [14,15].

Stirling engines have been studied over the years using different models [9,16]. Those have been solved analytically or numerically: (1) zero-order models based on experimentation [10]; (2) first-order models, corresponding to isothermal analysis (*Schmidt* analysis); (3) second-order models, accounting thermal and friction losses in addition to isothermal analysis [12]; (4) third-order modelling, considering *Navier Stokes* and energy conservation equations [11]; and more recently (5) models based on Computational Fluid Dynamics (CFD) [17,18]. Most of these studies are focused on the performance parameters such as power output, heat-exchangers effectiveness, overall efficiency, energy dissipation and heat losses, as studied by Hachem *et al.* [9] and Rogdakis *et al.* [10]. Others are based on the research of geometrical aspects such as the cylinders capacity, heater, cooler and regenerator configurations. Kongtragool and Wongwises [11] investigated the operational conditions by performing a sensitivity analysis of rotational speed, and mean pressure levels. Also, Thombare and Verma [19] concluded in their review that for good efficiency results, the design of heat exchangers and the proper selection of drive mechanism are needed. Timoumi *et al.* [20] evaluated the Stirling engine performance considering the effect of the physical and geometrical parameters and they have determined the optimal operational gas pressure. Valenti *et al.* [21] presented a numerical and experimental study about a commercial Stirling unit able to generate 1 kW of electricity and 8 kW of hot water. The model presented a good correlation with the experimental results. A net electrical output of 930 W was obtained for the CHP unit from experimental measurements, being very close to the simulated value of 941 W. Costa *et al.* [18] have computed a numerical procedure to characterize the pressure drop through the coiled wire mesh of a micro-CHP Stirling engine regenerator. Their study evidenced that the regenerator efficiency rises with mass flow rate increase, and that the efficiency is higher for the cooling process than for the heating. Several of these models using The optimization of the Stirling engines components configuration, *i.e.*, both operational and geometrical parameters, was already studied in previous work [13,22]. The Stirling engine optimization is a typical multi-objective optimization problem because there are *n*-dimensional variables to be evaluated. In multi-objective optimization, the decision-making process for selection of the best optimal solution is typically accomplished by programming techniques for multidimensional analysis or Pareto frontiers [23]. Once the best design is obtained, the thermo-economic analysis determines the average cost rates, the components cost or the specific cost per exergy unit of electricity [24]. Duan *et al.* [25] applied the particle swarm optimization algorithm to solve a thermo-economic to optimize thermal efficiency, engine power output, and the cycle irreversibility parameter simultaneously.

Stirling engines as prime movers run on fossil fuels. Nevertheless, Stirling engines have a high potential of using renewable energy sources with high overall efficiencies [10,26]. Mathematical models based on energy and economic parametrization and contemplating the use of Stirling engines using solar energy is also documented in the literature [27,28]. Due to the increased overall efficiency and losses minimization, Solar Dish Stirling (SDS) systems are an efficient technology to generate electricity using solar energy. Parameters such as the concentration ratio, hot and cold temperature, regenerator effectiveness, absorber temperature, working fluid have been considered for the performance analysis of SDS systems [13,29,30]. Singh and Kumar [31] performed a review and reported that the overall efficiency of a solar-dish Stirling system is reduced by nearly 25% if the regenerator losses are considered. Also, it is indicated that engines with higher regenerator effectiveness have higher thermal efficiency. Dadasaheb *et al.* [32] presented a study performing a second-order analysis for solar-powered beta Stirling engine. The authors wanted to investigate the most suitable operating temperature range so as to get the optimum value of the efficiency. They concluded that, for an overall efficiency between 25% and 27%, the optimum temperature range was of 750–1000 K. Bataineh [33] performed a study regarding the analysis of SDS engine using the non-linearized heat loss model of the solar dish collector and the irreversible cycle model of the Stirling engine. The study claims that the maximum thermal efficiency stated for SDS system is 32%, considering a concentration ratio of 1300 and an absorber temperature of 850 K. Nepveu *et al.* [34] developed a global thermal analysis of the energy conversion of a 10 kW_{el} Stirling unit coupled with a *Eurodish* collector. Andraka [35] developed a technical feasibility study of a dish-Stirling system with storage system incorporated. Li *et al.* [36] studied a strategy to improve the control of temperature at the heat absorber by implementing an adiabatic model of the engine. Gholamalizadeh and Chung [37] studied the influence of the aperture diameter and geometric concentration ratio in the design of the collector to improve the performance of the solar dish Stirling engine. Asnaghi *et al.* [38] simulated a solar Stirling system to study the impact of temperature difference of heater and cooler and regenerator volume in the work output and overall efficiency. Ehtiwesh *et al.* [39] presented a thermoeconomic analysis of a concentrated solar power plant, using the specific exergy cost to evaluate the environmental impact and cost, in terms of exergy for the entire life cycle of the plant. Ahmadi and his co-authors [40] presented the optimization of a solar-powered high-temperature differential Stirling engine considering multiple criteria. A thermal model was developed so that the output power and thermal efficiency of the solar Stirling system with finite rate of heat transfer, regenerative heat loss, conductive thermal bridging loss, finite regeneration process time and imperfect performance of the dish collector could be obtained. The problem was formulated as a multi-objective problem applying evolutionary algorithms based on the NSGA-II algorithm.

Table 1 summarizes several studies from the literature using solar Stirling. The specifications regarding the systems performance (e.g. power output, thermal and electrical efficiencies) and the operational parameters (*e.g.* rotation speed, driving mechanism, type of working gas and mean operating pressure) are provided.

Within the renewable energy sources, biomass has an important role, since several countries such as Portugal have an extensive forest area, whose products or residues can be valued as an energy source. A very interesting option is to use the forestry by-materials to produce pellets, particularly for the domestic sector. As a densified form of biomass, pellets are characterized by high

Table 1
Studies from the literature using Stirling engines to convert solar energy in power energy.

Author	Year	Type of work	Fuel	Micro-generation Unit	*Power output* (kW)	Working gas	*Pressure* (bar)	*Speed* (rpm)	*Hot Temperature* (K)	*Thermal efficiency* (%)	*Electrical efficiency* (%)
Bataineh [41]	2018	Numerical and Experimental	Solar radiation	Alpha−type differential Stirling with Ross Yoke mechanism	4.1	Hydrogen	2.0	3000	877	39.5	NA
Xiao et al. [42]	2018	Numerical and Experimental	Solar radiation	100W β-type Stirling engine	0.13	Helium	28.5	800	771	12.1	NA
Gholamalizadeh and Chung [37]	2017	Numerical and Experimental	Solar radiation	Kerman pilot parabolic dish with free piston	0.63−1.0	Helium	10	NA	800	17	NA
Kadri and Abdallah	2016	Numerical and Experimental	Solar radiation	Solar-driven Stirling heat engine system	1.3−2.5	Helium and Hydrogen	80	Variable speed	700−1150	NA	NA
Andraka [43]	2014	Numerical	Solar radiation	Solar-only Stirling dish with storage	25	NA	NA	NA	973−1073	NA	NA
Toghyani et al. [44]	2014	Numerical	Solar radiation	Optimization of a GPU3 Beta type Stirling	4.2	Helium	49.8	2500	939	29.7	NA
Li et al. [36]	2014	Numerical	Solar radiation	Dish-Stirling solar-thermal generation system	27	NA	200	1820	1033	NA	NA
Asnaghi et al. [38]	2012	Numerical	Solar radiation	SOLO 161 Solar Stirling engine	26.6	Helium	100	1800	923	26.9	NA
He and Sanders [45]	2011	Numerical and Experimental	Energy from a solar-thermal collector	Low-power engine prototype using a TES	2.5	Air	30	1200	453	21	NA
Nepveu et al. [34]	2009	Numerical	Solar radiation	Analysis of a SOLO Stirling 161	11.1	Hydrogen	130 −140	1500	1053	NA	21.6

NA - Not Available.

calorific value and low moisture content. This specific fuel can be converted into another form of useable energy for power and heat production by means of thermochemical conversion, such as direct combustion. These conversion technologies are coupled with other conversion technologies in order to produce electricity and heat. González *et al.* [46] and Martinez *et al.* [47] performed a very extensive review of the different technologies for small and micro-scale energy production of heat and power from biomass. Several of those studies use CFD tools to analyse the biomass combustion models. Farokhi [48] published a computational study to evaluate the influence of turbulence and combustion models in the performance of a small lab-scale biomass furnace (8−11 kW). Buczynski *et al.* [49] developed a CFD-based mathematical model to improve both the design and operation of the biomass-fuelled domestic boiler. An improved circular combustion chamber and a combustion air swirling were the most important outcomes from the boiler design optimization.

Over the past two decades, some biomass-fuelled Stirling engines have been designed, developed and tested in order to evaluate their performance [50,51]. One of the first works on this field was reported by Carlsen *et al.* [52] regarding the design of a four-cylinder Stirling engine with a maximum power of 40 kW adapted to the combustion of wood chips. Authors like Podesser [53] and Lane and Beale [54] developed and constructed a biomass Stirling engine in 1999. After this, in Austria, a 35 and 70 kW CHP Stirling engine system integrated with a wood chip boiler was run successfully for a long period of time [55,56]. Nishiyama *et al.* [57] combined a combustion chamber with a 55 kW_{el} Stirling engine unit, burning 0.03 kg/s of wood powder in the biomass combustion process. It was proved that wood powder has excellent properties as a fuel for Stirling engine CHP system.

Furthermore, some works focused on biomass micro-CHP systems. Dong *et al.* [58] provided an important review on the development of small- and micro-scale biomass-fuelled CHP systems. They have concluded that the constant rise in gas and electricity prices and the advances in the development of biomass-fuelled CHP technologies will increase their economic competitiveness. Thiers *et al.* [59] carried out an experimental observation on commercial 1.5 to 3 kW_{el} Stirling engine integrated with a wood pellets boiler in order to assess the performance specified by the manufacturer. The authors reported a lower power output and efficiency when compared with these reported by the manufacturer. Kölling *et al.* [60] combined a wood chip operated fire tube biomass boiler with an α-type Stirling SOLO 2V engine working with helium at 12 MPa and 900 K. According to their results, the system has a capacity to generate 4.5 kW_{el} of electricity and 12.7 kW_{th} of thermal power, if condensation and re-cooling techniques are considered. Cardozo *et al.* [61] also coupled a wood pellet burner and a gamma type Stirling engine. Results showed that overall efficiency reached a value of 72% and the authors also pointed out the importance of the position of the Stirling engine in relation to the burner. More recently, Cardozo *et al.* [62] reported the performance of a 20 kW residential boiler using wood and sugar cane bagasse pellets integrated with a 1 kW Stirling engine from *Genoastirling* [63]. The aim was to assess the effects of different pellets types, the combustion chamber length and operating cycle on the temperatures and how the thermal power is actually absorbed. The authors concluded that the position of the Stirling engine is highly relevant in order to use as much as possible of the radiative heat from the burner. Furthermore, also recently, several projects have studied the performance of this specific technology to produce heat and power through biomass use. In general, all of them were evaluated, designed, implemented and put into operation using prototypes or commercial devices [63–68]. The state-of-the-art of micro biomass CHP units using Stirling engine technology was reviewed and Table 2 presents the main research works in this area, as well as, important works in the small-scale applications.

Although pellets are considered a fuel with high availability and interesting properties to combustion, the development of small and micro-scale biomass-fuelled CHP systems suitable for application in domestic buildings is reduced and the systems commercially available are very limited [58,69]. This is primarily due to problems

Table 2
Studies from the literature using Stirling engines to convert biomass energy in power energy.

Author	Year	Type of work	Fuel	Micro-generation Unit	*Thermal output* (kW)	*Power output* (kW)	Working gas	*Pressure* (bar)	*Speed* (rpm)	*Hot Temperature* (K)	*Overall efficiency* (%)	*Electrical efficiency* (%)
Cardozo et al. [62]	2019	Experimental	Wood and sugar cane bagasse pellets	Experimental test rig	20	1	Nitrogen	15	NA	≈773	>83	>9
Sowale et al. [75]	2018	Numerical	Human wastes	Bench-scale downdraft combustor test rig	25	≈27.2	Helium	10	1431	663	NA	17.81
Schneider et al. [76]	2018	Description of a new Pilot CHP plant	Wood pellets, chips and biogenic products	Pilot plant with a SE from FTM	45–50	5	Helium	33	NA	NA	NA	25
Damirchi et al. [68]	2016	Experimental and Numerical	Agriculture wastes	Experimental test rig	NA	0.046 (max.)	Helium	3–10	400 – 700	643–683	NA	16 (max.)
Schnetzinger et al. [77]	2016	Experimental	Wood pellets	Biomass pellet burner prototype with a SE from FTM	NA	4–5	NA	NA	NA	≈923	NA	14.4–15.5
Cardozo et al. [61]	2014	Experimental	Wood pellets	Experimental test rig	≈15	0.46 –0.49	Nitrogen	12–25	NA	≈773	>72	≈3
Kölling et al. [78]	2014	Experimental (proof of concept)	Wood chips	KÖB boiler with SE SOLO 2V	12.7	4.5	Helium	120	NA	973	80	20
Senkel et al. [66,79]	2012	Experimental	Wood chips	KÖB boiler with SE SOLO 2V	12.7	4.5	Helium	120	NA	973	80	20
Renzi et al. [80]	2014	Numerical	Biogas	–	4.44	1	NA	NA	NA	773	90	22.5
Müller et al. [81]	2013	Experimental	Wood pellets	Fluidized bed facility with Sunmachine SE	15.5 and 16	2.05 and 2.45	Nitrogen	31 and 39	NA	NA	26.7 and 25.6	13.2 and 15.3
Marinitsch et al. [82]	2011	Experimental	Wood chips	Updraft gasification unit	141	22	Helium	46	1010	≈873	80.3	10.8
Thiers et al. [59]	2010	Experimental and Numerical	Wood pellets	Sunmachine Pellet micro-CHP unit test	≤5.4	≤1.38	Nitrogen	33–36	500 – 1000	873–1073	72.1	14.3
Biederman et al. [56]	2004	Experimental	Wood chips	small-scale CHP pilot plant	475	75	Helium	45	1000	NA	86	12
Biederman et al. [55]	2003	Experimental	Wood chips	small-scale CHP pilot plant	220	35	Helium	45	1010	953–1053	90	9.2
Podesser et al. [53]	1999	Experimental	Wood chips	Test biomass Stirling engine	12.5	3.2	Nitrogen	33	600	NA		25
Lane et al. [54]	1999	Description of a micro CHP system	Chunk wood and pellets	Prototype pellet burner (sunpower)	≈4	≈1	Helium	30	3000	823	>85	23

NA – Not Available, SE – Stirling Engine, FTM - Frauscher Thermal Motors.

related to the fuel ash content, such as fouling and slagging, and a low flue gas temperature close to the Stirling engine [70]. These are problems that, inevitably, lead to low specific power and efficiency.

Despite these facts, in the last decades, some companies like *Sunmachine* and *Sunpower* have developed micro-scale CHP systems and tried to commercialize their products (1 and 7.5 kW_{el}), but these products were discontinued [71]. More recently, an Austrian company, ÖkoFEN, had launched a pellet boiler coupled with a Stirling engine, *Pellematic Condens_e*, for a single-family dwelling. Its thermal output is up to 13 kW_{th} and the rated electrical capacity of the system corresponds to 600 W_{el} [72]. The pellet boiler was integrated with a free-piston Stirling engine built from *Microgen* [73]. *Qnergy* is another pellet-driven CHP plant with higher electrical and thermal output [74]. Table 3 and Table 4 present the technical specifications of the selected available commercial Stirling Engines for micro-CHP using biomass and the technical specifications of the biomass micro-CHP units for private households.

This paper aims to analyse the impact of two renewable energy sources in the performance of an alpha Stirling engine for small and micro-scale systems. The performance of the Stirling engine is assessed by comparing solar energy and biomass as external energy sources. Section two presents the mathematical model to conduct numerical simulations. The third section includes the modelling of the two renewable energy sources under study: the solar dish and

Table 3
Technical specifications of selected available commercial Stirling Engines for micro-CHP using biomass.

Unit	Model	Engine Type	*Thermal output* (kW)	*Electric Power* (kW)	Working gas	*Maximum Pressure* (bar)	*Speed* (rpm)	*Hot Temperature* (K)	*Electrical Efficiency* (%)
Disenco [83]	Inspirit 2.0	NA	10	2	NA	NA	NA	NA	NA
Disenco [83]	Inspirit 3.0	NA	15	3	NA	NA	NA	NA	NA
Microgen [73]	–	Free Piston	NA	1.05	NA	NA	NA	NA	26
Qnergy [74]	PCK80	Free Piston	25	7.1 (max.)	Helium	NA	NA	673–1073	30
Genoastirling [63]	ML3000	Gamma	18.6	3.3	Nitrogen	30	750	1123/1223	14
Genoastirling [63]	ML1000	Gamma	10	1.1	Nitrogen	30	750	1123/1223	14

Table 4
Technical specifications of the biomass micro-CHP units for private households.

Company	Micro-generation Unit	Fuel	*Thermal Output* (kW)	*Electric Power* (kW)	*Overall Efficiency* (%)	*Electrical Efficiency* (%)
ÖkoFEN (SE from Qnergy) [84]	Pellematic e-max	Wood pellets	50–60	4–5	93	7
ÖkoFEN (SE from Microgen) [72]	Pellematic Condens_e	Wood pellets	9–13	0.6	>90	6
Sunmachine[a] [59]	Sunmachine Pellet	Wood pellets	4.5–10.5	1.5–3	90	20–25

[a] Discontinued.

the biomass burner. In section four, the main results are presented and discussed, along with an economic analysis based on the levelized cost of energy. The last section is devoted to the conclusions which are summarized considering the mathematical modelling and the key findings.

2. Stirling engine modelling

A program-code was developed in the MatLab® environment to solve the thermal model of an alpha Stirling engine, a suitable technology for single and multi-family residential applications (1–50 kW_{el}). The code is based on several moduli, which allows different configurations of each mechanical component.

2.1. Stirling engine configuration

The alpha-Stirling configuration consists of two mechanically linked pistons located in separate cylinders (usually in a "*V*" configuration), which defines the compression and expansion spaces (the engine body). The working gas flows between these two spaces by alternate crossing of a low temperature heat exchanger (the cooler), a special heat exchanger containing a finely matrix of metal wires, which is able to absorb and release heat from and back to the working fluid (the regenerator) and a high temperature heat exchanger (the heater). Thus, the engine can be considered as a set of five components connected in series: the compression space (*c*), cooler (*k*), regenerator (*r*), heater (*h*) and the expansion space (*e*) [13]. The Stirling engine configuration considering all the main components is represented by Fig. 1.

The choice of this particular configuration is related to its lower mechanical losses when compared with gamma or beta configurations. The mechanical losses are mostly due to the roughness of cylinder surface, the difference between the diameter of the cylinder and piston rings, the variation of working gas mass between the inflow and outflow, as well, as the gap losses [85]. However, each Stirling configuration has different mechanical characteristics and, in alpha configuration, the displacer is not typically used. As the two pistons are in two separated cylinders, pistons move uniformly in the same direction to provide constant-volume heating cooling processes of the working fluid. When all the working fluid has been transferred into the cylinder, one piston is fixed and the other piston moves to expand or compress the working gas.

The heater is responsible for the heat transfer from the energy source to the operating fluid. This type of heat exchangers is not easy to define because of the distinct operation conditions inside and outside the exchanger. The inner surface is at high pressure and high temperature turbulent flow, whereas the outer surface is subjected to high temperature and steady low pressure flow [15]. On the other hand, the cooler absorbs heat from the working gas and rejects it to a coolant. Stirling engines are usually water-cooled, so the coolant should be at a low temperature because as the temperature increases, the thermal efficiency drops [86].

Based on these considerations, the heater and the cooler were defined as a bundle of thin pipes. This configuration was chosen due to the need of: (*i*) a large contact area to improve the heat transfer process; and (*ii*) a large mass flow of working gas with low pressure. The regenerator has a tubular configuration with a wired mesh, which is able to absorb and release heat from and back to the working gas. Helium was used as the working fluid due to its thermal properties. It has a higher thermal diffusivity and dynamic viscosity than hydrogen, despite its lower thermal conductivity [87,88]. Previous studies also proved that the engine specific power is roughly proportional to the engine speed and mean pressure [87,88]. Thus, the mean operating pressure varies between 5 and

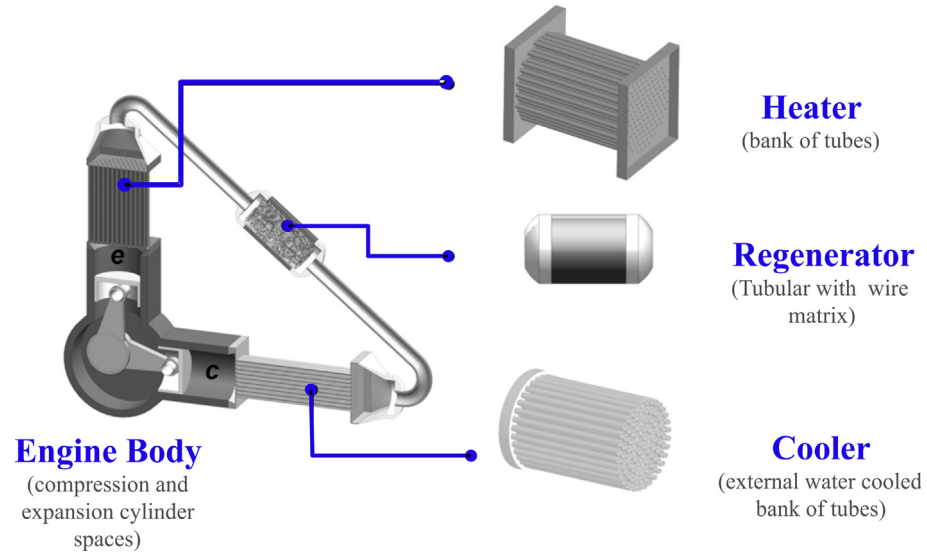

Fig. 1. Representation of the Stirling engine configuration considering: the engine block, the heater, the cooler and the regenerator geometrical arrangement. Adapted from Ref. [13].

80 bar and the rotational speed was defined to be a constant value, 1500 rpm. The geometric characteristics of cooler, regenerator and heater, as well as the cylinders volumes and other operating input parameters, are shown in Table 5.

2.2. Stirling mathematical modelling

Each component represents an entity endowed with its respective volume (V), temperature (T), absolute pressure (P) and mass (m). Enthalpies flowing across the interfaces/boundaries depend on the adjacent upstream temperatures and mass flows. Thus, heat is transferred from the external heat source through the heater walls, whereas the convective losses are calculated and the temperature of the working gas is estimated. At the regenerator, heat is cyclically stored and recovered and the fluid temperature is calculated iteratively. The working gas temperature in the cooler is evaluated by calculating the overall heat transfer coefficient, which includes: the convective heat transfer from the cooler tubes to the working fluid; the conduction through the cooler tubes' walls; and the convective heat transfer to an external mass flow of coolant (useful heat). Fig. 2 illustrates the heat transfer process between two subsequent components, the compression space and the cold heat exchanger (cooler).

Thus, the mathematical model integrates a two-step calculation procedure. The first analysis is an ideal adiabatic simulation, which provides the initial condition for the non-ideal simulation. The algorithm iteratively invokes the ideal adiabatic code and, at each time-step, new values for the temperature of the working gas for the heater (T_h) and cooler (T_k) are calculated, until convergence is attained. After each simulation run, the values of heat that are transferred into the heater (Q_h) and cooler (Q_k) are determined. The heat reversely transferred between the regenerator matrix and the

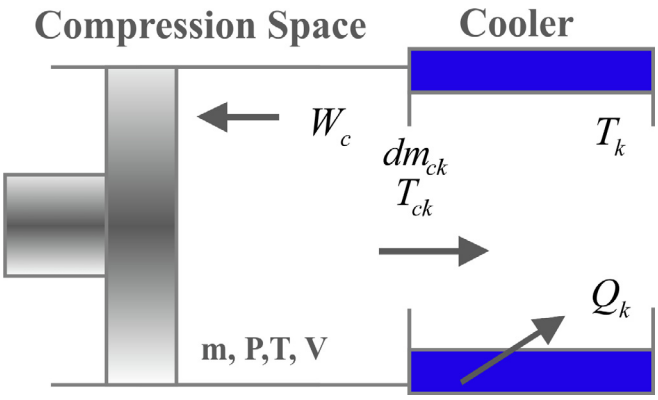

Fig. 2. Example of the heat transfer process between the compression space and cooler. It represents the energy transferred at each heat exchanger, which can be calculated considering the temperature and mass flow at the boundary between two subsequent components.

Table 5
Input operational and geometric parameters for simulations.

Parameter of each engine component	Value
Engine Cylinders (Pistons, compression and expansion spaces)	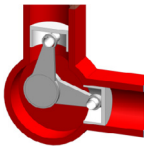
Phase angle (configuration) [°]	90 (Sinusoidal)
Engine swept volume [cm^3]	130.0
Engine clearance volume [cm^3]	25.0
Engine rotational speed [rpm]	1500
Mean operating pressure [bar]	5–80
Regenerator (Tubular Regenerator with wire matrix)	
Regenerator Length (L_r) [mm]	60.0
Matrix Porosity ($\varphi_{r,matrix}$)[–]	0.7
Wire Matrix Diameter ($d_{r,wire}$) [mm]	0.3
Regenerator Volume (V_r) [cm^3]	69.8
Heater (Arrangement of smooth pipes)	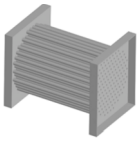
Heater Length (L_h) [mm]	150.0
Number of Tubes (nt_h) [–]	80
Heater volume (V_h) [cm^3]	84.8
Cooler (Bundle of parallel smooth tubes)	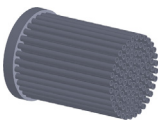
Cooler Length (L_k) [mm]	100.0
Number of Tubes (nt_k) [–]	150
Cooler volume (V_k) [cm^3]	106.0

working gas can also be estimated ($Q_{r,ideal}$). Subsequently, the non-ideal analysis integrates the effects of non-perfect regeneration and pumping losses. The non-perfect regeneration is due to the convective thermal resistance between the regenerator surface and the working gas, while the gap and pumping losses refer to sealing problems and fluid friction, respectively. As a result, there is a pressure drop and, consequently, a reduction of the power output. Thus, seven ordinary differential equations are iteratively solved, in which the initial values of all the variables are arbitrated and the equations are integrated from the initial state over a complete cycle, including:

1. The reduction of heat transfer in the regenerator ($Q_{r,loss}$), which is quantified as a function of the effectiveness of the regenerator and the ideal adiabatic conditions;
2. The net engine work per cycle is calculated as a function of expansion and compression volumes, and the work loss per cycle due to the pressure drops in the three heat exchangers.

Fig. 3 presents a simplified flowchart of the calculation algorithm. However, the full numerical model description is presented elsewhere [13,89,90].

3. External energy sources modelling

The performance of the Stirling engine is assessed by comparing solar energy and biomass as external energy sources. In this section, the solar collector dish and the biomass boiler modelling are presented. Both numerical models were coded and implemented in MatLab® language.

3.1. Solar collector dish modelling

The solar energy source was modelled as a concentric solar dish. The design of a concentric solar collector and its cavity receiver require solving a mathematical model that takes into account the optical, geometric and thermal characteristics of the physical components. The receiver is typically located at the focal point, which is designed to absorb the solar radiation for transferring the heat energy to the working fluid of the Stirling engine. Its configuration aims to minimize thermal losses. The energy available to the Stirling engine (Q_{engine}) is calculated as the difference between the heat in the receiver cavity ($Q_{receiver}$) and the emissivity losses ($Q_{losses,\ emissivity}$) and the convection losses ($Q_{losses,\ conv}$). The heat delivered to the receiver cavity is calculated as a function of the solar irradiation average value ($\bar{I}_{receiver}$) and the receiver area ($A_{receiver}$), as in (1).

$$Q_{receiver} = \bar{I}_{receiver} A_{receiver} \tag{1}$$

A fraction of the energy entering the receiver cavity returns to the surroundings through the cavity opening. The heat losses due to the surface emissivity (δ), can be calculated as a function of Stefan-Boltzmann constant (σ), the receiver area ($A_{receiver}$), the average temperature at the receiver ($T_{receiver}$) and the ambient temperature (T_{amb}) as in (2). According to Ref. [91] it is acceptable assuming the receiver with an emissivity of 1.0, as considered in this model.

$$Q_{losses,\ emiissivity} = \delta\, \sigma A_{receiver} \left(\bar{T}^4_{receiver} - T^4_{\mathrm{amb}} \right) \tag{2}$$

The convection heat losses determination requires the calculation of the convection heat transfer coefficient in the cavity receiver ($h_{receiver}$) as a function of the Nusselt number ($\mathrm{Nu_D}$), the thermal conductivity (k) and the receiver diameter ($D_{receiver}$). $\mathrm{Nu_D}$ is derived from the correlation of Churchill and Bernstein [92] regarding the heat transfer in cylinders as in (3),

$$Nu_D = 0.3 + \frac{0.62 \mathrm{Re}^{1/2} \mathrm{Pr}^{1/3}}{\left[1 + \left(0.4 \mathrm{Pr}^{2/3}\right)\right]^{1/4}} \left[1 + \left(\frac{\mathrm{Re}}{282000} \right)^{5/8} \right]^{4/5} \tag{3}$$

where Re and Pr are the Reynolds and Prandtl numbers, respectively. To calculate the heat losses by convection, wind velocity of 3.0 m/s was assumed and the Prandtl number was assumed to be 0.7. Thus, the convection heat losses, $Q_{losses,\ conv}$, are calculated as in (4).

$$Q_{losses,\ conv} = h_{receiver} A_{receiver} (\bar{T}_{receiver} - T_{amb}) \tag{4}$$

Several optical and geometrical parameters have to be defined in order to calculate the mean temperature within the receiver cavity: the dish diameter, the distance from the aperture for which

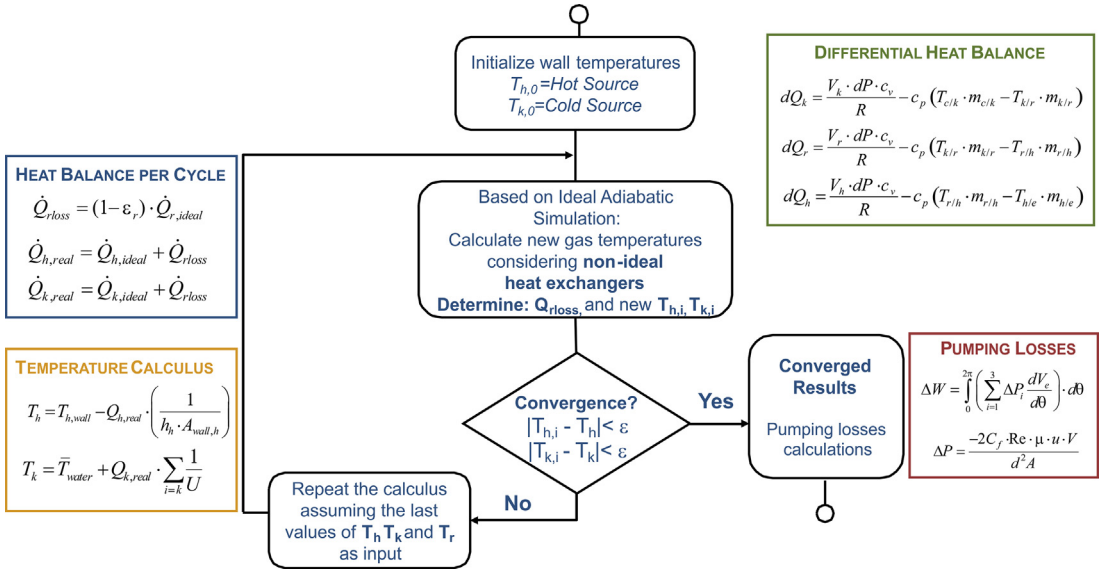

Fig. 3. Flow diagram of the calculation algorithm.

the solar image fits the absorber area; the incident and rim angle and materials reflectance [93].

Table 6 presents the operating conditions and dimensional variables used to evaluate numerically the thermal performance of the cavity receiver. A constant rim angle of 45° and an incidence angle of 23° were assumed [93]. In Portugal, there is a significant potential in terms of global solar radiation, due to the considerable number solar hours, which range from 2200 to 3000 on annual basis [94]. Thus, for simulation purposes, a constant input for the solar irradiation in collector varies between 500 and 900 W/m^2 and an ambient temperature of 298 K was assumed. These values took into consideration the local climate conditions in Portugal [95].

3.2. Biomass boiler modelling

3.2.1. Combustion test facility

Fig. 4 presents the experimental set-up located in the *Laboratory of Energy and Fluids* in the *Mechanical Engineering Department* at the University of Minho (Portugal). In brief, the combustion facility is composed of a pellet boiler and gas analysis unit. The boiler works under forced draught and its operation was programmed with *LabVIEW National Instruments*, automatically regulating the airflow rate by adjusting the fan speed. The feeding rate is adjusted through the screw feeder movement.

The flue gases are forced to exit the boiler through a fan and, in doing so, fresh air enters the combustion chamber, due to the induced pressure gradient, by the primary and secondary air channels. Heat is dissipated in a cooling loop. The primary air channel introduces the air into the bottom of the grate through 28 orifices, with rectangular section, and some air is also introduced through 48 circular orifices, just above the bottom. The secondary air channel introduces the air through 36 orifices. To initiate the combustion, the pellets are supplied from the top of the grate by the screw and the ignition is accomplished with the aid of an electrical resistance placed on the grate. In this way, the combustion of the pellets takes place within the grate and the flue gases released dissipate energy through a heat exchanger before being released to the exhaust stack. The boiler has a 20 kW of thermal power with 50% of excess air ratio.

Table 7 presents the nominal operating conditions of this experimental facility. The fuel employed in this specific unit is the commercial-grade A1 pinewood pellets, with 6 mm of diameter produced from pine sawdust.

Table 8 shows the pellet ultimate and proximate analysis. The analysis resulted from an extensive study of the pellets composition and the values were obtained from experimental measurements [98]. The proximate analysis was performed according to standards CEN/TS 15414:2006, CEN/TS 15402:2006, and CEN/TS 15403:2006. The ultimate analysis was performed according to standard CEN/TS 15104 and the sulphur was measured according to standard CEN/TS 15408 by a Leco TruSpec Series. The heat value measurement was performed according to the procedures specified in the CEN/TS 14918:2005 standard and it was measured by a calorimeter Leco AC500.

Table 6
Design parameters of the concentric solar dish collector [13,93,96].

Design Parameter	Value
Dish diameter [m]	8.0
Receiver aperture diameter [m]	0.12
Reflectance [−]	0.94
Rim angle [°]	45.0
Incident angle [°]	23.0
Optical total error [mrad]	8.0

3.2.2. Numerical model

Data from the biomass conversion, taking place in the boiler bed of the test facility, were used as input for the numerical model implemented in MatLab®. The process of biomass combustion in the bed is a complex process that consists in numerous consecutive homogeneous and heterogeneous reactions: heating-up, drying, devolatilization (producing char and volatiles), volatiles and char combustion compounds [99]. It is assumed that combustion starts with the ignition on the bed' surface and, when a fuel particle enters in a furnace, it dries and devolatilizes, mainly through thermal radiation. Thus, a simple bed model is proposed, based on the research from Porteiro [100]. The model computes the temperature of the flue gases leaving the bed through an energy balance, considering the energy introduced into the bed ($\dot{E}_{in}$), the energy that is provided by the bed ($\dot{E}_{out}$), and the incident radiation in the bed ($\dot{Q}_{rad}$). This energy balance can be expressed as in (5).

$$\dot{E}_{in} + \dot{Q}_{rad} - \dot{E}_{out} = 0 \quad (5)$$

Regarding the energy introduced into the bed, it is composed of the dry fuel, fuel moisture and air supply to the boiler. In terms of energy, the formation enthalpies of different compounds are used under standard conditions. In relation to the energy provided by the bed, as a result of the reactions that take place in the bed, an empirical model that computes the mass fraction of volatile gases as a function of the temperature is considered [101]. This empirical model is useful as a subroutine to determine the biomass combustion products because it is often difficult to measure the volatile products. This is important to determine the quantity of energy released through the main volatile gases produced during the devolatilization of the biomass. Furthermore, it is also considered the energy released from the char combustion and the remaining air. Finally, the radiation heat is based on the difference between the incident radiation from the combustion chamber and the radiation from the bed to the combustion chamber. Thus, this energy balance in the bed takes into account important input parameters: (*i*) fuel properties, (*ii*) fuel mass flow rate, (*iii*) air supply, (*iv*) radiation received from the combustion chamber and (*v*) boiler operating conditions.

4. Results and discussion

In this section, the numerical results are presented and discussed. The first two subsections concern the results of a sensitivity analysis of the operational parameters of the solar dish and biomass combustion that directly influence the performance of Stirling engine. The third subsection presents the main results from the Stirling engine comparing the two renewable energy sources. Finally, a brief economic analysis is presented in the fourth section.

4.1. Sensitivity analysis to the solar dish parameters

The design procedure of the solar collection system (dish-cavity) starts with a geometrical-optical performance evaluation of the concentrator. The greatest advantage of solar collectors lies on its concave reflecting surface able to focus the solar irradiation to a much smaller receiving area, resulting in increased heat flux [31]. Thus, the heat flux depends on the aperture diameter, which can be correlated with several parameters of the dish design. According to Ferreira *et al.* [93] the aperture diameter of the cavity is equal to the width of the solar image produced in the focal plane. In turn, the solar image can be estimated considering the optical errors, distance from the concentrator surface to the focal point and the number of standard deviations for the radiation beam entering the receiver cavity. Fig. 5 depicts a sensitivity analysis of the solar image width as

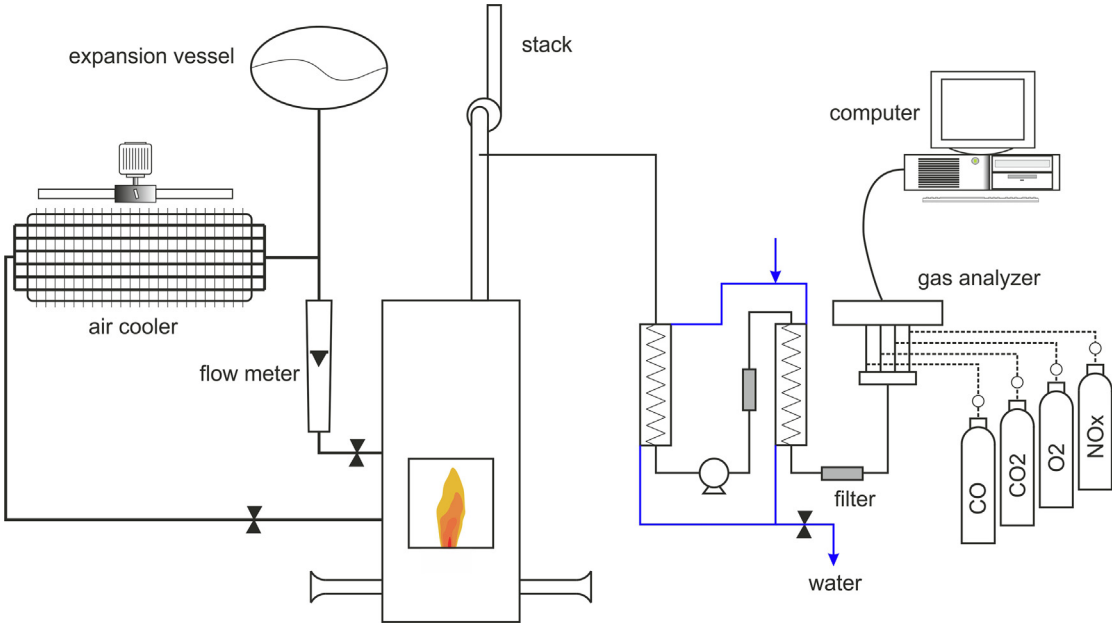

Fig. 4. Layout of the test combustion facility.

Table 7
Operating conditions of a 20 kW Pellet Boiler [97].

Parameter	Value
Air temperature [K]	298
Fuel flow rate [kg/h]	4.30
Fuel temperature [K]	298
Primary air mass flow rate [m^3/h]	30.4
Secondary air mass flow rate [m^3/h]	59.6
Excess air [%]	50

Table 8
Ultimate and proximate analysis of the fuel used in this work.

Proximate analysis (wt.%, as received)		Ultimate analysis (wt.%, dry ash free)	
Moisture	6.90	Carbon	50.90
Volatile matter	77.80	Hydrogen	5.39
Ash	0.60	Nitrogen	1.55
Fixed carbon	14.70	Sulphur	0.037
LHV [MJ/kg]	17.10	Oxygen	42.22

a function of the total rim for different values of total angular errors. Higher values of the solar image width require higher rim angles in order to capture the same amount of solar radiation.

The reflected radiation that passes into the cavity receiver depends on the aperture ratio and rim angle. A dish with a very small rim angles has very little curvature, and the focal point and the receiver must be placed far from the concentrator surface, increasing the thermal losses. For this reason an aperture of 0.12 m was considered a reasonable value. This value is in agreement with the results from Beltran *et al.* [96], who concluded that the efficiency and heat transfer to the Stirling reaches their maximum point when the aperture diameter is equal to 0.13 m. The same authors also stated that the optimal optic behaviour is achieved for cavities with an aperture diameter near 0.13 m a rim angle of 45° and when the solar radiation ranges between 700 W/m^2 and 1000 W/m^2. Based on these results, a solar radiation of 900 W/m^2 and the total optical error of 8 mrad were considered to run the simulations.

As shown in Fig. 6, concentric solar dishes with a rim angle starting at 45° have lower focal distances and consequently, lower aperture ratios. For these conditions, a higher fraction of reflected radiation passes to the receiver cavity of the Dish Stirling system, independently of the dish diameter. Thus, it focuses the solar irradiation to a much smaller receiving area, resulting in an increased heat flux.

Fig. 7 presents the variation of the average temperature at the receiver ($T_{receiver}$) and the variation of the optic concentration ratio (C_f) as a function of the dish diameter (D_{dish}). These two variables are deeply related and both have an exponential increase for higher diameters of the solar dish. The reason is related to the fact that the concentration of solar flux is not uniformly distributed over the receiver aperture area ($A_{receiver}$) and, in fact, high and low flux levels are distributed around the receiver aperture area. As a result, the optic concentration ratio is lower than the geometrical ratio, and the quotient represents the way to measure the amount of energy available transmitted to the receiver, with certain solar collection efficiency. These considerations were also verified by Beltran *et al.* [96], who have studied a parabolic dish concentrator coupled with a Stirling engine.

Based on all these considerations, a solar dish with 8 m of diameter and a fixed rim angle of 45° were assumed for the analysis. This configuration allows achieving a mean temperature in the receiver of 1009 K and almost 30 kW of heat transferred to the engine.

Similar results were obtained by Dadasaheb et al. [32] who have investigated the operating temperature range of solar dishes. They concluded that the optimum temperature is in the range of 750–1000 K.

4.2. Sensitivity analysis of the biomass boiler parameters

In this section, a validation of the bed model is presented. The model presents a wide versatility since it allows defining important parameters as the radiation flux from the combustion chamber and the percentage of air supplied in the bed. This study evaluates the effect of these parameters on the temperature of the flue gases. For this purpose, the radiation received onto the fuel surface was

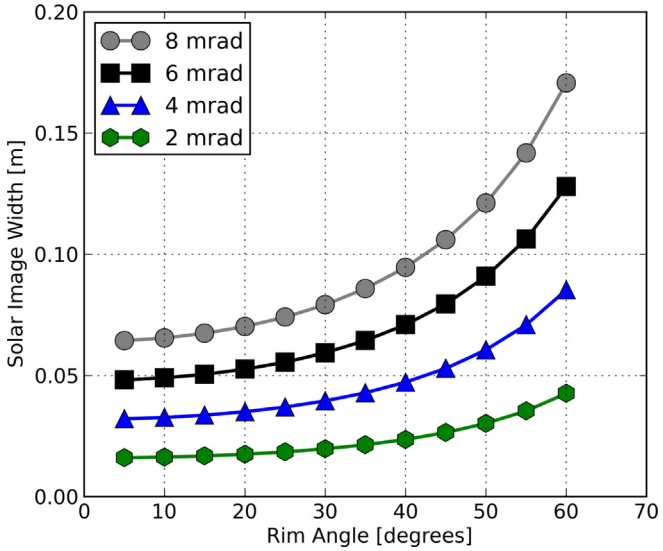

Fig. 5. Solar image with as a function of rim angle for different values of total optical error.

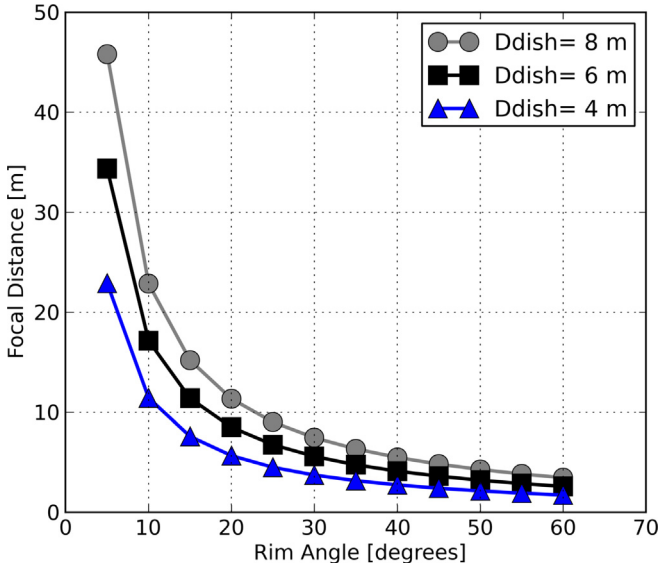

Fig. 6. Focal distance as a function of rim angle for different solar dish diameters.

estimated through previous studies in a 20 kW pellet boiler from the Mechanical Engineering Department at the University of Minho [97]. Furthermore, the boiler operating conditions and fuel properties were also based on the same boiler [97,102].

A sensitivity analysis regarding the most important parameters affecting the temperature inside the boiler was carried out. Fig. 8 presents the flue gases temperature obtained with the bed model as a function of three different values of the radiation flux and different percentage of air supplied in the bed. As expected, the temperature of the flue gases increases with the increasing the radiation flux, and decreases for higher split percentages between the primary air and secondary air. From the analysis, a value of 1288 K was considered to run the numerical simulations. Similar results were obtained by Peters [103], who have achieved temperature values of approximately 1200 K, for comparable values of heat flux (1.3 E+5 W/m^2).

4.3. Results from Stirling engine performance

The factors that mostly affect the engine efficiency are the hot and cold source temperatures, heat-transfer limitations and the pumping losses. Thus, in the optimal design of Stirling engines, the three heat-exchangers characteristics are crucial, namely the compromise between their thermal efficiency and the power output. The thermal losses are due to the pressure gradient required to move the working fluid through the three heat exchangers (mainly the flow through the regenerator).

All these effects were considered in the non-ideal analysis, and numerical simulations were carried out considering helium as the working fluid. Table 9 presents the results corresponding to simulations performed at 1500 rpm and with mean cycle gas pressures of 50 bar considering both renewable energy sources. The results show that the biomass provides much higher power and work per cycle than solar energy. In fact, assuming the same operating and geometrical parameters, the biomass-fuelled Stirling engine provides 87.5% more power than the solar one. This outcome is due to the difference between the amount of heat that is actually transferred from the hot heat source to the Stirling receiver. For both models, the thermal losses are relatively low.

While the average receiver temperature from the solar source is about 775 K, at the boiler bed, the temperature is around 1288 K. Thus, when using a biomass-fuelled Stirling engine, a system with a 4.3 kW of power output was obtained. The biomass-fuelled Stirling allows reaching relatively high values for the engine total efficiency, of about 46.67%, when compared to an efficiency of 31.33% for the Stirling solar dish technology. The effectiveness of the heat exchangers is an important parameter, which influences the cycle thermal efficiency. The regenerator effectiveness is the highest when compared to that of the hot and cold exchangers, reaching values of 92.60% for the biomass-fuelled Stirling. In fact, it was already proved by other authors that the engine performance worsens when the heat-transfer capacity of the regenerator declines and it is very sensitive to it [104].

The mean operating pressure is one of the operational parameters that most affect the Stirling engine specific power and efficiency. Engines operating at higher mean pressures represent larger costs in terms of materials, but provide systems with considerably higher outputs. Fig. 9 presents the variation of the power output and Fig. 10 presents the engine efficiency variation, both as a function of the mean pressure.

As expected, higher operating pressures correspond to higher values of power output produced by the system and it is easily observed that it increases almost linearly with the mean pressure. Additionally, for pressures above 30 bar, the difference between the two systems in terms of power output is significant (biomass-fuelled system produces more 80% than the solar-powered system).

Regarding the influence of the mean operation pressure on engine efficiency, it was verified a decay of efficiency with increasing mean pressure. This outcome may be related to the heat transfer limitations (reduction in the effectiveness of all heat-exchangers). Cardozo et al. [105] experimentally evaluated the integration of an overfed wood pellet burner and a prototype Stirling engine, concluding that the thermal power absorbed by the Stirling engine increases with the temperature on the hot side. For the same range of temperatures, higher pressures also lead to higher thermal power absorbed by the engine. Higher pressure inside the Stirling engine has a positive effect on the thermal power output.

Table 10 presents the results of the average gas temperature inside the heater and cooler, obtained from the non-ideal analysis at a rotational speed of 1500 rpm and a mean pressure of 5 and 80 bar. The average gas temperature inside the heater is directly affected by the input heat source. In the specific case of solar-

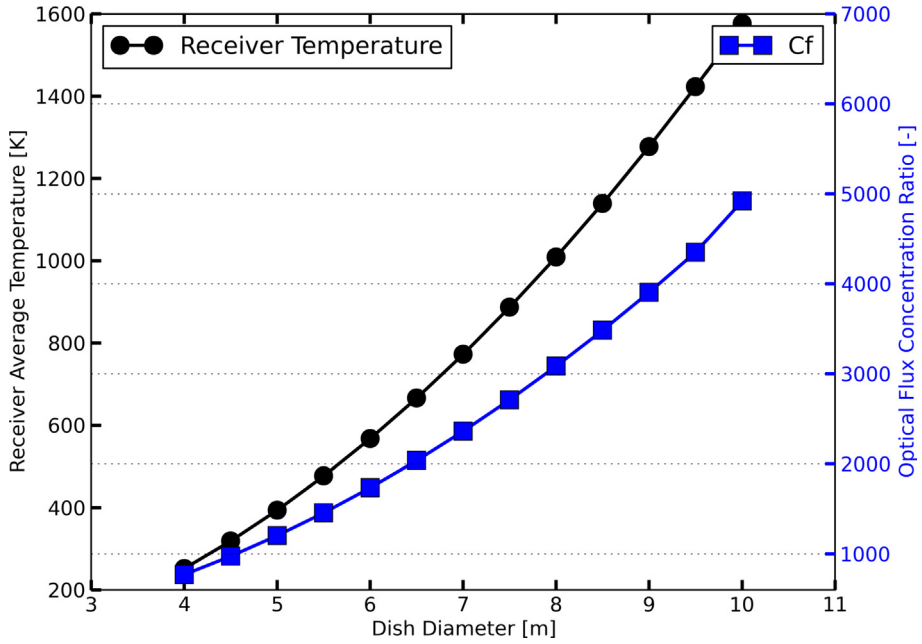

Fig. 7. Receiver Average temperature and optic concentration ratio (C_f) as a function of the rim angle for different values of dish diameter.

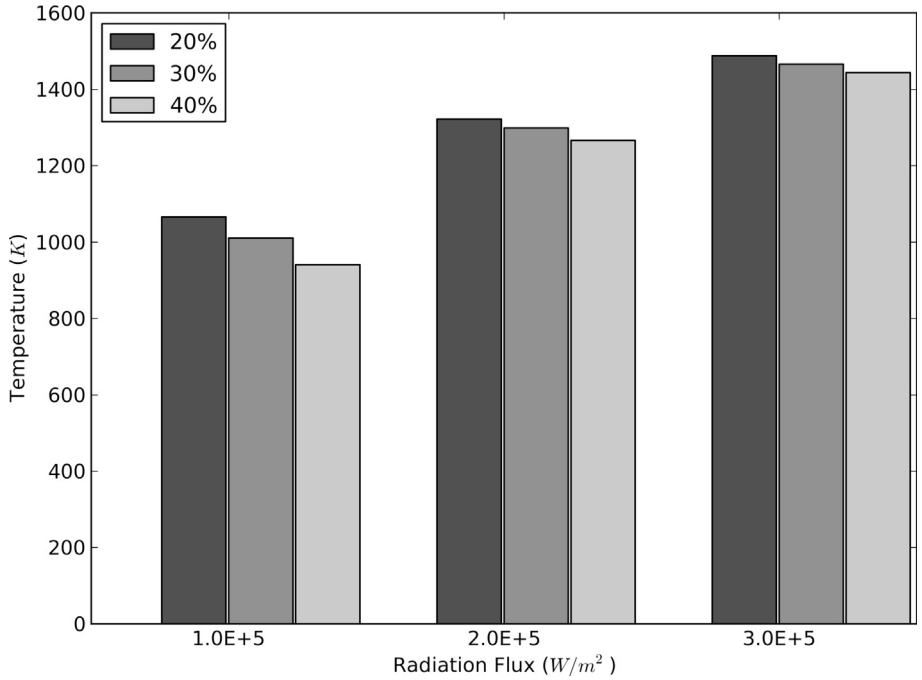

Fig. 8. Temperature variation for different values of radiation flux considering different percentages of primary split air (40%, 30% and 20%).

powered system, the maximum temperature reached in the absorber inside the receiver is limited mainly by the convective and radiation losses, which justifies a lower temperature value transferred to the working gas inside the heater.

In the case of biomass-fuelled system, the thermal losses are lower, so the average temperature is closer to the flue gases temperature obtained with the bed model. Concerning the average gas temperature in the cooler, the results are not so different when comparing the solar-powered with the biomass-fuelled system. The effect of the pressure in the temperature variation is mostly related to the thermal properties of the working fluid.

4.4. Economic analysis

The Levelized Cost of Energy (LCoE) is an economic indicator used, to calculate the minimum cost of energy supplied by a system or a technology, representing a profit breakeven point. This indicator comprises economic considerations such as initial investment, installation costs, maintenance and operating costs, feed-in-tariffs, interest rates, technical lifetime and depreciation. As a comprehensive economic indicator, LCoE can be used to compare results from different technological solutions as in the case of the present study [106].

Table 9
Results from the non-ideal analysis considering a rotational speed of 1500 rpm and a mean pressure of 50 bar considering the solar and biomass energy sources.

Parameter	Solar-powered system	Biomass fuelled system
Real Hot source heat, Q_h [J]	293.04	368.68
Real Cold source heat, Q_k [J]	201.60	197.04
Work [J]	91.80	172.08
Power [W]	2295	4302
Work Losses [W]	4.53	3.822
Thermal Efficiency [%]	40.51	61.75
Total Efficiency [%]	31.33	46.67
Regenerator Effectiveness [%]	84.40	92.60
Heater Effectiveness [%]	53.41	59.58
Cooler Effectiveness [%]	39.28	40.41

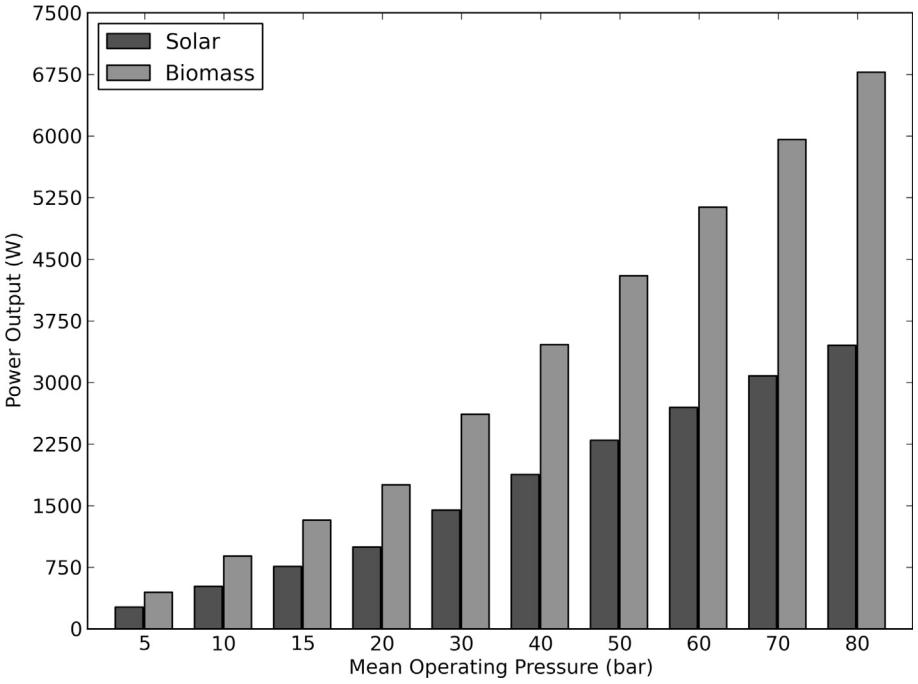

Fig. 9. Power output as a function of the mean pressure at 1500 rpm.

The manufacturing and operating costs can be calculated and distributed into annuities over the technical lifetime of the thermal system, considering the annual depreciation. In order to compare energy conversion units, technical and investment costs were obtained directly from commercial manufacturers and suppliers.

Solar dish Stirling systems investments are deeply related to the number of systems manufactured. The specific investment of a 10 kW solar dish unit, considering a concentrator with 8.5 m of diameter is approximately 4200 €/kW, including assembly and engineering costs, as well as the support structure, tracking mechanisms and foundations. Since such systems are mostly installed in areas of high direct radiation, a full 2400 load hours per year can be considered [37]. For this technology and system scale, the maintenance and operating costs can be estimated as about 1.5% of the investment costs. The technical and economic data of a 10 kW solar dish Stirling system is presented in Table 11.

Regarding the biomass-fuelled system, the costs were based on a commercial 20 kW wood pellet boiler. The costs involved in producing energy included the investment costs with the equipment, installation, operational and maintenance costs. The investment costs include the boiler, the pellet feeder and the storage acquisition cost. The system installation consists of piping material cost (e.g. system piping, insulation material and system components cost such as pumps, valves. The maintenance cost for a modern wood pellet boiler comprises cleaning at the end of each heating season to avoid pellet fines accumulation, combustion conditions verification and ash disposal. According to Wang *et al.* [107], the total maintenance cost can be assumed as 1% of the total investment cost of biomass boilers. The operational cost comes directly from fuel consumption. The fuel cost comes from the consumption of wood pellets, which is a factor of the consumption rate and the fuel price. Based on the literature, these systems operate for a period of 7000 h per year. The specific investment, considering a boiler's pellet feed rate of 12.98 kg/h corresponds to 1063.4 €/kW. The technical and economic data of the biomass boiler integrated with a Stirling engine is presented in Table 12.

The total accumulated operating time for the Stirling engines is about 180 000 h, corresponding to 20.5 years [13]. Thus, the economic analysis was conducted considering a technical lifetime of 20 years for both systems. The initial capital costs are annualized as if it were being paid off a loan at a particular interest of discount rate over the lifetime of the option. The capital recovery factor is used to determine the equal amounts of n cash transactions for the investment, depending on the effective rate of return. The effective

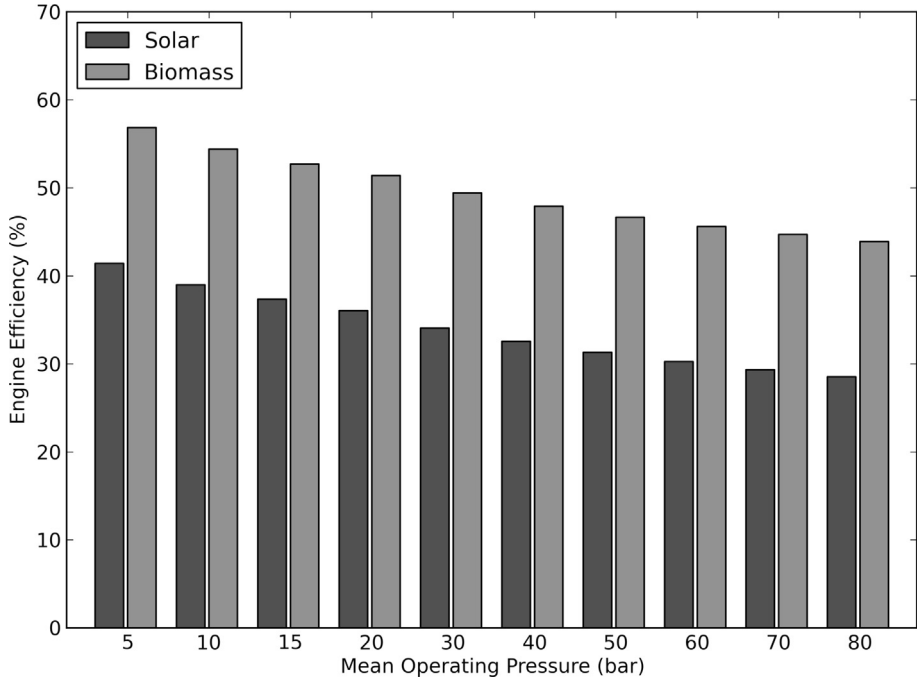

Fig. 10. Engine efficiency as a function of the mean pressure at 1500 rpm.

Table 10
Heater and cooler average gas temperature results from the non-ideal analysis considering a rotational speed of 1500 rpm at a mean pressure of 5 and 80 bar.

Parameter	Solar-powered system		Biomass-fuelled system	
Operating Pressure [bar]	5	80	5	80
Heater average gas temperature [K]	751.6	722.6	1243	1205
Cooler average gas temperature [K]	338.0	383.1	367.9	400.3

rate of return, $i_e = 4.5\%$, can be approximated as the interest rate, minus the inflation rate plus owners' risk factor. The Levelized Cost of Energy (LCoE) can be estimated as in (6). Table 13 presents the calculated LCoE values and the specific investment costs for both systems under study.

$$LCoE = \frac{C_{inv} \cdot \frac{i(1+i)^n}{(1+i)^n - 1}}{System\ \ Capacity \cdot t} + \frac{C_{O\&M} + C_{fuel}}{\text{Energy Produced}} \quad (6)$$

Considering the outlined reference investment costs and technical considerations, the minimum cost of energy is of about 0.166 €/kWh with the solar-powered system, which is relatively higher than the biomass-fuelled system (0.109 €/kWh). Despite the considerable weight of biomass fuel cost, the investment cost of solar dish Stirling is too high to compensate for the lower costs with the operational and maintenance costs as well as the lack of fuel expenses. The result is also explained with the number of operating hours of each system, since the solar-powered system is limited by the solar radiation availability to operate.

5. Conclusions

This paper presented an analysis regarding the impact of different renewable energy sources, *i.e.* solar energy and biomass, in the performance of an alpha Stirling engine for small scale systems. A two-step numerical model of an alpha-Stirling engine was implemented in MatLab. Stirling engines were used in the study because of their technical specifications and because they are a suitable technology for single and multi-family residential applications (1–50 kW_{el}). In this research work:

- The performance of the Stirling engine is assessed by comparing solar energy and biomass as external energy sources;
- The heat transfer process from the solar energy to the Stirling receiver was modelled considering a concentric solar dish with a diameter of 8 m, an aperture of 12 cm and the solar radiation varying between 500 and 900 W/m^2;

Table 11
Technical and economic data of a 10 kW solar dish Stirling system [13,37].

Technical and economic data		Solar-powered system
Technical data	System capacity [kW]	10
	Dish Diameter, D_{dish} [m]	8.5
	Full-Load Working hours, t [h/year]	2400
	Technical lifetime, n [years]	20
Investment and Operational Costs	Investment Capital Costs, C_{inv} [€]	42 000
	Dish mirror, structure, foundations	25 000
	Stirling engine and receiver	11 000
	Installation	6000
	Operating and Maintenance Costs, $C_{O\&M}$ [€/year]	750

Table 12
Technical and economic data of a 25 kW biomass boiler with a Stirling [105,107].

Technical and economic data		Biomass-fuelled system
Technical data	System capacity [kW]	20
	Pellet feed rate, $\dot{m}_{pellets}$ (kg/h)	12.8
	Full-Load Working hours, t [h/year]	7000
	Technical lifetime, n [years]	20
Investment and Operational Costs	Investment Capital Costs, C_{inv} [€]	26 590
	Boiler and Pellet Feeder	12 440
	Stirling engine	11 000
	Pellet Storage and System components	3150
	Operating and Maintenance Costs, $C_{O\&M}$ [€/year]	2659
	Fuel Costs, C_{fuel} [€/year]	14 336

Table 13
Results of specific investment cost and levelized cost of energy for both systems.

	Solar-powered system	Biomass-fuelled system
Specific investment cost [€/kW]	4200.0	1063.4
LCoE [€/kWh]	0.166	0.109

- The combustion process in the boiler bed and the respective energy balance was modelled considering the fuel properties and mass flow rate, the air supply, the radiation flux inside the combustion chamber and the boiler operating conditions.
- Simulations were carried out considering the operating and geometrical parameters of the Stirling engine and its thermal components for both energy inputs.

The main results and key findings led to the conclusion that:

- The biomass-fuelled Stirling engine provided 87.5% more power output than the solar energy source. It provides a power output of 4.3 kW with a total efficiency of 46.67%, whereas the solar system results in a system with 2.30 kW of power with an efficiency of 31.33%. These results show that the energy source plays an important role and results in different engine performances.
- The average receiver temperature from the solar source is about 775 K, whereas, in the boiler bed, the temperature reaches the value of 1288 K.
- In the solar-powered system, the reflected radiation that passes into the cavity receiver depends on the aperture ratio and rim angle. It was proved that a rim angle of at least 45° is required to ensure lower focal distances. Otherwise, the Stirling receiver needs to be placed far from the surface of the dish, resulting in higher thermal losses and lower temperature inside the receiver cavity.
- In biomass-fuelled system, it was shown that the temperature of the flue gases increases with the radiation flux increasing, and decreases for higher split percentages between the primary air and secondary air. Some issues especially regarding the combustion stability due to particle emission in the flue gas and reduced temperature close to the Stirling engine need to be solved. Thus, the flame temperature should be considered in boiler modelling in order to improve the Stirling performance.
- The LCoE for the solar-power system is of about 1658 €/kWh, which is 52% higher when compared with the biomass-fuelled system (0.109 €/kWh).
- With increasing concerns over environmental issues, particularly with the increasing levels of CO_2 in the atmosphere, the use of renewable energy sources embrace the great potential in the world. Biomass is a good option because it avoids the problems usually associated with solar energy intermittency and its use at domestic installations is significant.

Despite the significant results, the mathematical model needs some improvements concerning the heat transfer, gap, hysteresis and pressure loss effects in the Stirling engine. The integration of all these aspects makes the thermodynamic model more realistic in determining the effective temperatures of the working gas within each operating component and the reduction of thermodynamic efficiency. Also, as future work, exergy analysis of both alternative systems should be included in order to provide more inclusive results of the systems performance evaluation.

Declaration of competing interest

The authors declare that they have no known competing financial interests or personal relationships that could have appeared to influence the work reported in this paper.

CRediT authorship contribution statement

Ana Cristina Ferreira: Writing - original draft, Formal analysis, Software. **João Silva:** Writing - original draft, Formal analysis, Software. **José Carlos Teixeira:** Supervision, Funding acquisition. **Silvia Azucena Nebra:** Supervision.

Acknowledgements

The first author would like to express her gratitude for the support given by the Portuguese Foundation for Science and Technology (FCT) through the Post-Doc Research Grant SFRH/BPD/121446/2016. This work has been supported by FCT within the R&D Units Project Scope UIDB/00319/2020 (ALGORITMI) and R&D Units Project Scope UIDP/04077/2020 (METRICS).

Nomenclature

A	area, m^2
C	cost, €
C_f	concentration ratio
c	compression space
c_p	specific heat at constant pressure, $kJ.kg^{-1}K^{-1}$
c_v	specific heat at constant volume, $kJ.kg^{-1}K^{-1}$

CFD	computational fluid dynamics
CHP	combined heat and power
D	dish diameter, m
$d_{r,wire}$	matrix wire diameter, mm
E	energy flux, W/m^2
e	expansion space
i_e	effective rate of return, %
$\bar{I}$	incident radiation flux W/m^2
h	heater
k	cooler
L	tubes length, mm
LCoE	levelized cost of energy
m	Mass of working gas, kg
$\dot{m}$	mass flow, kg/h
n	number of years
nt	number of tubes
Nu	Nusselt Number
P	pressure, bar
ΔP	pressure drop, bar
Pr	Prandtl Number
Q	thermal energy, J/cycle
$\dot{Q}$	thermal power, J/cycle
$Q_{r,ideal}$	adiabatic heat transferred at regenerator matrix, J/cycle
Q_{rloss}	heat-transfer Reduction at Regenerator, J/cycle
R	gas constant, $kJ.kg^{-1}K^{-1}$
r	regenerator
Re	Reynolds Number
SDS	solar dish stirling
T	temperature, K
t	working hours, h
u	velocity, m/s
V	volume, cm^3
W	work, J/cycle
ΔW	work loss, J/cycle

Greek symbols

k	thermal conductivity, W/(mK)
ε	effectiveness, %
δ	emissivity
θ	increment angle, °
σ	Stefan-Boltzmann constant
φ	regenerator matrix porosity
μ	dynamic viscosity, kg.m^{-1}.s^{-1}

Subscripts and superscripts

amb	ambient condition
conv	convective
el	electrical
engine	refers to engine
f	refers to fuel
h	refers to heater
in	refers to inflow
inv	refers to investment costs
k	refers to cooler
loss	refers to heat losses
losses, conv	refers to convection losses
losses, emissivity	refers to emissivity losses
matrix	refers to regenerator matrix
O&M	refers to operational and maintenance costs
out	refers to outflow
pellet	refers to pellet
rad	radiation flux
real	refers to real values of non-ideal analysis
receiver	refers to collector receiver
th	thermal
wall	refers to component wall
wire	refers to regenerator matrix wire

References

[1] V. Kuhn, J. Klemeš, I. Bulatov, MicroCHP: Overview of selected technologies, products and field test results, Appl. Therm. Eng. 28 (2008) 2039–2048, https://doi.org/10.1016/j.applthermaleng.2008.02.003.

[2] D. Connolly, H. Lund, B.V. Mathiesen, Smart Energy Europe: the technical and economic impact of one potential 100% renewable energy scenario for the European Union, Renew. Sustain. Energy Rev. 60 (2016) 1634–1653, https://doi.org/10.1016/j.rser.2016.02.025.

[3] Directive 2012/27/Eu, Energy efficiency directive 2012/27/EU of the European parliament and of the council. http://ec.europa.eu/energy/efficiency/eed/eed_en.htm, 2012.

[4] M. Bianchi, A. De Pascale, P.R. Spina, Guidelines for residential micro-CHP systems design, Appl. Energy 97 (2012) 673–685, https://doi.org/10.1016/j.apenergy.2011.11.023.

[5] K. Alanne, N. Söderholm, K. Sirén, I. Beausoleil-Morrison, Techno-economic assessment and optimization of Stirling engine micro-cogeneration systems in residential buildings, Energy Convers. Manag. 51 (2010) 2635–2646, https://doi.org/10.1016/j.enconman.2010.05.029.

[6] M. Badami, F. Camillieri, A. Portoraro, E. Vigliani, Energetic and economic assessment of cogeneration plants: a comparative design and experimental condition study, Energy 71 (2014) 255–262, https://doi.org/10.1016/j.energy.2014.04.063.

[7] K. Alanne, A. Saari, Sustainable small-scale CHP technologies for buildings: the basis for multi-perspective decision-making, Renew. Sustain. Energy Rev. 8 (2004) 401–431, https://doi.org/10.1016/j.rser.2003.12.005.

[8] M.C.C. Campos, J.V.C.V.C. Vargas, J.C.C. Ordonez, Thermodynamic optimization of a Stirling engine, Energy 44 (2012) 902–910, https://doi.org/10.1016/j.energy.2012.04.060.

[9] H. Hachem, R. Gheith, F. Aloui, S. Ben Nasrallah, Technological challenges and optimization efforts of the Stirling machine: a review, Energy Convers. Manag. 171 (2018) 1365–1387, https://doi.org/10.1016/j.enconman.2018.06.042.

[10] E.D. Rogdakis, G.D. Antonakos, I.P. Koronaki, Thermodynamic analysis and experimental investigation of a Solo V161 Stirling cogeneration unit, Energy 45 (2012) 503–511, https://doi.org/10.1016/j.energy.2012.03.012.

[11] B. Kongtragool, S. Wongwises, Thermodynamic analysis of a Stirling engine including dead volumes of hot space, cold space and regenerator, Renew. Energy 31 (2006) 345–359, https://doi.org/10.1016/j.renene.2005.03.012.

[12] P. Puech, V. Tishkova, Thermodynamic analysis of a Stirling engine including regenerator dead volume, Renew. Energy 36 (2011) 872–878, https://doi.org/10.1016/j.renene.2010.07.013.

[13] A.C. Ferreira, M.L. Nunes, J.C.F. Teixeira, L.A.S.B. Martins, S.F.C.F. Teixeira, Thermodynamic and economic optimization of a solar-powered Stirling engine for micro-cogeneration purposes, Energy 111 (2016) 1–17, https://doi.org/10.1016/j.energy.2016.05.091.

[14] M.H. Ahmadi, M.A. Ahmadi, A. Mellit, F. Pourfayaz, M. Feidt, Thermodynamic analysis and multi objective optimization of performance of solar dish Stirling engine by the centrality of entransy and entropy generation, Int. J. Electr. Power Energy Syst. 78 (2016) 88–95, https://doi.org/10.1016/j.ijepes.2015.11.042.

[15] A.C. Ferreira, S.F.C.F. Teixeira, J.C. Teixeira, L.A. Barreiros Martins, Parametric analysis of the thermal components of an alpha-stirling engine for cogeneration applications, in: Energy, American Society of Mechanical Engineers, Tampa, vol. 6, 2017, https://doi.org/10.1115/IMECE2017-71313. V006T08A011.

[16] B. Kongtragool, S. Wongwises, A review of solar-powered Stirling engines and low temperature differential Stirling engines, Renew. Sustain. Energy Rev. 7 (2003) 131–154, https://doi.org/10.1016/S1364-0321(02)00053-9.

[17] A.K. Almajri, S. Mahmoud, R. Al-Dadah, Modelling and parametric study of an efficient Alpha type Stirling engine performance based on 3D CFD analysis, Energy Convers. Manag. 145 (2017) 93–106, https://doi.org/10.1016/j.enconman.2017.04.073.

[18] S.C. Costa, H. Barrutia, J.A. Esnaola, M. Tutar, Numerical study of the heat transfer in wound woven wire matrix of a Stirling regenerator, Energy Convers. Manag. 79 (2014) 255–264, https://doi.org/10.1016/j.enconman.2013.11.055.

[19] D.G. Thombare, S.K. Verma, Technological development in the Stirling cycle engines, Renew. Sustain. Energy Rev. 12 (2008) 1–38, https://doi.org/10.1016/j.rser.2006.07.001.

[20] Y. Timoumi, I. Tlili, S. Ben Nasrallah, Design and performance optimization of GPU-3 Stirling engines, Energy 33 (2008) 1100–1114, https://doi.org/10.1016/j.energy.2008.02.005.

[21] G. Valenti, P. Silva, N. Fergnani, G. Di Marcoberardino, S. Campanari, E. Macchi, Experimental and numerical study of a micro-cogeneration stirling engine for residential applications, Energy Procedia 45 (2014) 1235–1244, https://doi.org/10.1016/j.egypro.2014.01.129.

[22] A.C. Ferreira, M.L. Nunes, L.B. Martins, S.F. Teixeira, Thermal analysis and cost estimation of Stirling cycle engine, WSEAS Trans. Power Syst. 9 (2014)

341–351. https://www.semanticscholar.org/paper/Thermal-Analysis-and-Cost-Estimation-of-Stirling-Ferreira-Nunes/69df7f254bc6e59169fdf495f1f08956bcb85c4b.
[23] M.H. Ahmadi, A.H. Mohammadi, S.M. Pourkiaei, Optimisation of the thermodynamic performance of the Stirling engine, Int. J. Ambient Energy 37 (2016) 149–161, https://doi.org/10.1080/01430750.2014.907211.
[24] M.H. Ahmadi, M.-A. Ahmadi, F. Pourfayaz, Thermal models for analysis of performance of Stirling engine: a review, Renew. Sustain. Energy Rev. 68 (2017) 168–184, https://doi.org/10.1016/j.rser.2016.09.033.
[25] C. Duan, X. Wang, S. Shu, C. Jing, H. Chang, Thermodynamic design of Stirling engine using multi-objective particle swarm optimization algorithm, Energy Convers. Manag. 84 (2014) 88–96, https://doi.org/10.1016/j.enconman.2014.04.003.
[26] B. Thomas, Benchmark testing of Micro-CHP units, Appl. Therm. Eng. 28 (2008) 2049–2054, https://doi.org/10.1016/j.applthermaleng.2008.03.010.
[27] S. Pavlovi, D. Vasiljevi, V. Stefanovi, E. Petrovi, Optical design of a solar parabolic concentrating collector based on trapezoidal reflective petals, J. Energy Power Eng. (2013) 1–5.
[28] J.H. Shazly, A.Z. Hafez, E.T. El Shenawy, M.B. Eteiba, Simulation, design and thermal analysis of a solar Stirling engine using MATLAB, Energy Convers. Manag. 79 (2014) 626–639, https://doi.org/10.1016/j.enconman.2014.01.001.
[29] R. Arora, S.C. Kaushik, R. Kumar, R. Arora, Multi-objective thermo-economic optimization of solar parabolic dish Stirling heat engine with regenerative losses using NSGA-II and decision making, Int. J. Electr. Power Energy Syst. 74 (2016) 25–35, https://doi.org/10.1016/j.ijepes.2015.07.010.
[30] G. Barreto, P. Canhoto, Modelling of a Stirling engine with parabolic dish for thermal to electric conversion of solar energy, Energy Convers. Manag. 132 (2017) 119–135, https://doi.org/10.1016/j.enconman.2016.11.011.
[31] U.R. Singh, A. Kumar, Review on solar Stirling engine: development and performance, Therm. Sci. Eng. Prog. 8 (2018) 244–256, https://doi.org/10.1016/j.tsep.2018.08.016.
[32] D.J. Shendage, S.B. Kedare, S.L. Bapat, Numerical investigations on the Dish–Stirling engine system, Int. J. Ambient Energy 40 (2019) 274–284, https://doi.org/10.1080/01430750.2017.1388840.
[33] K.M. Bataineh, Optimization analysis of solar-powered average temperature Stirling heat engine, J. Energy South Afr. 26 (2017) 55–66, https://doi.org/10.17159/2413-3051/2015/v26i1a2221.
[34] F. Nepveu, A. Ferriere, F. Bataille, Thermal model of a dish/Stirling systems, Sol. Energy 83 (2009) 81–89, https://doi.org/10.1016/j.solener.2008.07.008.
[35] C.E. Andraka, Dish stirling advanced latent storage feasibility, Energy Procedia 49 (2014) 684–693, https://doi.org/10.1016/j.egypro.2014.03.074.
[36] Y. Li, S.S. Choi, C. Yang, Dish-Stirling solar power plants: modeling, Analysis, and Control of receiver temperature, IEEE Trans. Sustain. Energy. 5 (2014) 398–407, https://doi.org/10.1109/TSTE.2013.2291572.
[37] E. Gholamalizadeh, J.D. Chung, Exergy analysis of a pilot parabolic solar dish-stirling system, Entropy 19 (2017) 509, https://doi.org/10.3390/e19100509.
[38] A. Asnaghi, S.M. Ladjevardi, P. Saleh Izadkhast, a.H. Kashani, Thermodynamics performance analysis of solar stirling engines, ISRN Renew. Energy. (2012) 1–14, https://doi.org/10.5402/2012/321923 (2012).
[39] I.A.S. Ehtiwesh, M.C. Coelho, A.C.M. Sousa, Exergetic and environmental life cycle assessment analysis of concentrated solar power plants, Renew. Sustain. Energy Rev. 56 (2016) 145–155, https://doi.org/10.1016/j.rser.2015.11.066.
[40] M.H. Ahmadi, M.A. Ahmadi, F. Pourfayaz, M. Bidi, H. Hosseinzade, M. Feidt, Optimization of powered Stirling heat engine with finite speed thermodynamics, Energy Convers. Manag. 108 (2016) 96–105, https://doi.org/10.1016/j.enconman.2015.11.005.
[41] K.M. Bataineh, Numerical thermodynamic model of alpha-type Stirling engine, Case Stud. Therm. Eng. 12 (2018) 104–116, https://doi.org/10.1016/j.csite.2018.03.010.
[42] G. Xiao, Y. Huang, S. Wang, H. Peng, M. Ni, Z. Gan, Z. Luo, K. Cen, An approach to combine the second-order and third-order analysis methods for optimization of a Stirling engine, Energy Convers. Manag. 165 (2018) 447–458, https://doi.org/10.1016/j.enconman.2018.03.082.
[43] C.E. Andraka, Dish stirling advanced latent storage feasibility, Energy Procedia 49 (2014) 684–693, https://doi.org/10.1016/j.egypro.2014.03.074.
[44] S. Toghyani, A. Kasaeian, M.H. Ahmadi, Multi-objective optimization of Stirling engine using non-ideal adiabatic method, Energy Convers. Manag. 80 (2014) 54–62, https://doi.org/10.1016/j.enconman.2014.01.022.
[45] M. He, S. Sanders, Design of a 2.5kW low temperature stirling engine for distributed solar thermal generation, in: 9th Annu. Int. Energy Convers. Eng. Conf., American Institute of Aeronautics and Astronautics, Reston, Virigina, 2011, pp. 1–8, https://doi.org/10.2514/6.2011-5508.
[46] A. González, J.-R. Riba, R. Puig, P. Navarro, Review of micro- and small-scale technologies to produce electricity and heat from Mediterranean forests' wood chips, Renew. Sustain. Energy Rev. 43 (2015) 143–155, https://doi.org/10.1016/J.RSER.2014.11.013.
[47] S. Martinez, G. Michaux, P. Salagnac, J.-L. Bouvier, Micro-combined heat and power systems (micro-CHP) based on renewable energy sources, Energy Convers. Manag. 154 (2017) 262–285, https://doi.org/10.1016/J.ENCONMAN.2017.10.035.
[48] M. Farokhi, M. Birouk, F. Tabet, A computational study of a small-scale biomass burner: the influence of chemistry, turbulence and combustion sub-models, Energy Convers. Manag. 143 (2017) 203–217, https://doi.org/10.1016/j.enconman.2017.03.086.
[49] R. Buczyński, R. Weber, A. Szlęk, Innovative design solutions for small-scale domestic boilers: combustion improvements using a CFD-based mathematical model, J. Energy Inst. 88 (2015) 53–63, https://doi.org/10.1016/j.joei.2014.04.006.
[50] M. Salomón, T. Savola, A. Martin, C.-J. Fogelholm, T. Fransson, Small-scale biomass CHP plants in Sweden and Finland, Renew. Sustain. Energy Rev. 15 (2011) 4451–4465, https://doi.org/10.1016/J.RSER.2011.07.106.
[51] E.S. Barbieri, P.R. Spina, M. Venturini, Analysis of innovative micro-CHP systems to meet household energy demands, Appl. Energy 97 (2012) 723–733, https://doi.org/10.1016/j.apenergy.2011.11.081.
[52] H. Carlsen, N. Ammundsen, J. Traerup, 40 kW Stirling engine for solid fuel, in: IECEC 96. Proc. 31st Intersoc. Energy Convers. Eng. Conf., IEEE, n.d.: pp. 1301–1306. doi:10.1109/IECEC.1996.553904.
[53] E. Podesser, Electricity production in rural villages with a biomass stirling engine, Renew. Energy 16 (1999) 1049–1052.
[54] N. Lane, W. Beale, A biomass-fired 1 kWe stirling engine generator and its applications in South Africa, in: 9th Int. Stirling Engine Conf., South Africa, 1999, p. 7.
[55] F. Biedermann, H. Carlsen, M. Schöch, I. Obernberger, Small-scale CHP plant based on a 35 kWel hermetic four cylinder stirling engine for biomass fuels-development, technology and operating experiences, in: Int. Nord. Bioenergy Conf. - Bioenergy 2003, Jyväskylä, Finland, 2003.
[56] F. Biedermann, H. Carlsen, I. Obernberger, M. Schöch, Small-scale CHP plant based on a 75 kWel hermetic eight cylinder stirling engine for biomass fuels - development, technology and operating experiences, in: 2nd World Conf. Exhib. Biomass Energy, Ind. Clim. Prot., Rome, Italy, 2004.
[57] A. Nishiyama, H. Shimojima, A. Ishikawa, Y. Itaya, S. Kambara, H. Moritomi, S. Mori, Fuel and emissions properties of Stirling engine operated with wood powder, Fuel 86 (2007) 2333–2342, https://doi.org/10.1016/j.fuel.2007.01.040.
[58] L. Dong, H. Liu, S. Riffat, Development of small-scale and micro-scale biomass-fuelled CHP systems – a literature review, Appl. Therm. Eng. 29 (2009) 2119–2126, https://doi.org/10.1016/j.applthermaleng.2008.12.004.
[59] S. Thiers, B. Aoun, B. Peuportier, Experimental characterization, modeling and simulation of a wood pellet micro-combined heat and power unit used as a heat source for a residential building, Energy Build. 42 (2010) 896–903, https://doi.org/10.1016/j.enbuild.2009.12.011.
[60] A. Kölling, W. Siemers, U. Hellwig, N. Sachno, S. Schröder, N. Senkel, High temperature biomass fired stirling engine (HTBS), Renew. Energy Power Qual. J. 1 (2014) 365–369, https://doi.org/10.24084/repqj12.341.
[61] E. Cardozo, C. Erlich, A. Malmquist, L. Alejo, Integration of a wood pellet burner and a Stirling engine to produce residential heat and power, Appl. Therm. Eng. 73 (2014) 671–680, https://doi.org/10.1016/J.APPLTHERMALENG.2014.08.024.
[62] E. Cardozo, A. Malmquist, Performance comparison between the use of wood and sugarcane bagasse pellets in a Stirling engine micro-CHP system, Appl. Therm. Eng. 159 (2019) 113945, https://doi.org/10.1016/J.APPLTHERMALENG.2019.113945.
[63] Genoastirling Genoastirling. https://genoastirling.com/eng/our-engines-characteristics.php, 2019.
[64] G. Qiu, Y. Shao, J. Li, H. Liu, S.B. Riffat, Experimental investigation of a biomass-fired ORC-based micro-CHP for domestic applications, Fuel 96 (2012) 374–382, https://doi.org/10.1016/j.fuel.2012.01.028.
[65] W.H. Rosemarie Schnetzinger, Stefan Aigenbauer, Christine Mair, Ernst Höftberger, Weissinger Alexander, Christoph Schmidl, Development of combustion concept for biomass pellet driven Stirling engine, in: 24th Eur. Biomass Conf. Exhib., Amsterdam, The Netherlands, 2016.
[66] N. Senkel, W. Siemeers, Combining solid biomass combustion and stirling technology, in: 20th Eur. Biomass Conf. Exhib., Milan, Italy, 2012.
[67] I. Arashnia, G. Najafi, B. Ghobadian, T. Yusaf, R. Mamat, M. Kettner, Development of micro-scale biomass-fuelled CHP system using stirling engine, Energy Procedia 75 (2015) 1108–1113, https://doi.org/10.1016/j.egypro.2015.07.505.
[68] H. Damirchi, G. Najafi, S. Alizadehnia, R. Mamat, C.S. Nor Azwadi, W.H. Azmi, M.M. Noor, Micro Combined Heat and Power to provide heat and electrical power using biomass and Gamma-type Stirling engine, Appl. Therm. Eng. 103 (2016) 1460–1469, https://doi.org/10.1016/j.applthermaleng.2016.04.118.
[69] D. Maraver, A. Sin, J. Royo, F. Sebastián, Assessment of CCHP systems based on biomass combustion for small-scale applications through a review of the technology and analysis of energy efficiency parameters, Appl. Energy 102 (2013) 1303–1313, https://doi.org/10.1016/j.apenergy.2012.07.012.
[70] I. Obernberger, Trends and opportunities of micro-CHP technologies based on biomass combustion, in: 18th Eur. Biomass Conf. Lyon 2010, Lyon, 2010, pp. 1–9. http://bioenergy2020.eu/files/publications/pdf/Obernberger-2010-Lyon-Micro-CHP.pdf.
[71] H. Liu, Biomass fuels for small and micro combined heat and power (CHP) systems: resources, conversion and applications, in: Small Micro Comb. Heat Power Syst, Elsevier, 2011, pp. 88–122, https://doi.org/10.1533/9780857092755.1.88.
[72] ÖkoFEN, ÖkoFEN - Pellematic Condens_e. http://www.okofen-e.com/en/pellematic_condens_e/, 2019.
[73] Microgen, Microgen Engine, 2019. https://www.microgen-engine.com/.
[74] Qnergy Qnergy. https://www.qnergy.com/, 2019.

[75] A. Sowale, A.J. Kolios, B. Fidalgo, T. Somorin, A. Parker, L. Williams, M. Collins, E. McAdam, S. Tyrrel, Thermodynamic analysis of a gamma type Stirling engine in an energy recovery system, Energy Convers. Manag. 165 (2018) 528–540, https://doi.org/10.1016/J.ENCONMAN.2018.03.085.
[76] J.K.T. Schneider, D. Müller, Biomass conversion with a fluidized bed-fired stirling engine in a micro-scale CHP plant, in: 26th Eur. Biomass Conf. Exhib. 14-17 May 2018, Copenhagen, Denmark, Copenhagen, Denmark, 2018, p. 5.
[77] E.H. Rosemarie Schnetzinger, Stefan Aigenbauer, Christine Mair, Development of combustion concept for biomass pellet driven stirling engine, in: 24th Eur. Biomass Conf. Exhib. 6-9 June 2016, Amsterdam, The Netherlands, 2016, p. 2.
[78] A. Kölling, W. Siemers, U. Hellwig, N. Sachno, S. Schröder, N. Senkel, High temperature biomass fired stirling engine (HTBS), in: Int. Conf. Renew. Energies Power Qual., Cordoba, Spain, 2014, p. 5.
[79] N. Senkel, W. Siemers, Combining solid biomass combustion and stirling technology, in: 21st Eur. Biomass Conf. Exhib., Copenhagen, Denmark, 2013, p. 5.
[80] M. Renzi, C. Brandoni, Study and application of a regenerative Stirling cogeneration device based on biomass combustion, Appl. Therm. Eng. 67 (2014) 341–351, https://doi.org/10.1016/j.applthermaleng.2014.03.045.
[81] J. Müller, D. Karl, Biomass CHP with micro-fluidized-bed combustion, in: 21st Eur. Biomass Conf. Exhib. 3-7 June 2013, Copenhagen, Denmark, 2013, p. 7.
[82] G. Marinitsch, J. Bovin, T. Gørtz, K. Mygind, H. Carlsen, CO2 neutral, low emission small scale biomass CHO plants based on updraft gasification and stirling engines – technology development, in: 19th Eur. Biomass Conf. Exhib., Berlim, Germany, 2011, p. 10.
[83] Disenco, Disenco - the inspirit charger. https://www.powerengineeringint.com/2008/01/08/disenco-announces-stirling-engined-micro-chp-roll-out/, 2019.
[84] ÖkoFEN, ÖkoFEN - Pellematic e-max. http://www.okofen-e.com/en/pellematic_e_max/, 2019.
[85] J. ŠKORPÍk, A leakage of piston rings and their impact on work Stirling engine, in: 14th Int. Stirling Engine Conf., Groningen–Netherlands, 2009, pp. 1–10.
[86] A.C.M. Ferreira, M.L. Nunes, L.B. Martins, S.F. Teixeira, Analysis of the geometrical parameters of thermal components in a stirling engine, in: 11th World Congr. Comput. Mech. WCCM 2014, 5th Eur. Conf. Comput. Mech. ECCM 2014 6th Eur. Conf. Comput. Fluid Dyn. ECFD 2014, International Center for Numerical Methods in Engineering, 2014, pp. 3734–3745. http://www.scopus.com/inward/record.url?eid=2-s2.0-84923972706&partnerID=tZOtx3y1.
[87] A.C. Ferreira, S. Teixeira, J.C. Teixeira, M.L. Nunes, L.B. Martins, Modeling a stirling engine for cogeneration applications, in: Vol. 6 Energy, Parts A B, ASME, Houston, USA, 2012, p. 361, https://doi.org/10.1115/IMECE2012-88183.
[88] A.C. Ferreira, S. Teixeira, C. Ferreira, J. Teixeira, M.L. Nunes, L.B. Martins, Thermal- economic modeling of a micro-CHP unit based on a stirling engine, ASME Int. Mech. Eng. Congr. Expo. Proc. (2013), https://doi.org/10.1115/imece2013-65126.
[89] A.C. Ferreira, S. Teixeira, M.L. Nunes, L.B. Martins, Numerical study of regenerator configuration in the design of a stirling engine, in: ASME (Ed.), Proc. ASME 2014 Int. Mech. Eng. Congr. Expo. IMECE2014, ASME, Montereal, Canada, 2014, https://doi.org/10.1115/IMECE2014-38529. V06AT07A021; 10 pages.
[90] A.C. Ferreira, M.L. Nunes, J.C.F. Teixeira, L.A.S.B. Martins, S.F.C.F. Teixeira, S.A. Nebra, Design of a solar dish Stirling cogeneration system: application of a multi-objective optimization approach, Appl. Therm. Eng. 123 (2017) 646–657, https://doi.org/10.1016/j.applthermaleng.2017.05.127.
[91] N. Sendhil Kumar, K.S. Reddy, Numerical investigation of natural convection heat loss in modified cavity receiver for fuzzy focal solar dish concentrator, Sol. Energy 81 (2007) 846–855, https://doi.org/10.1016/j.solener.2006.11.008.
[92] J.H. Lienhard, J.H. IV, V. Lienhard, A Heat Transfer Textbook, fifth ed., Dover Publications, Mineola, NY, 2001. http://ahtt.mit.edu.
[93] A.C. Ferreira, S. Teixeira, J.C. Teixeira, L.B. Martins, Design optimization of a solar dish collector for its application with stirling engines, in: 6A Energy, ASME, Houston, USA, Vol, 2015, https://doi.org/10.1115/IMECE2015-52241. ASME V06AT07A033.
[94] L. Gil, L. Basilio, I. Cabrita, G. Torres, M.R. Costa, Situação do solar térmico em Portugal, Renov. Mag. - Rev. Técnico-Profissional Energias Renov. 30 (2017) 48–52.
[95] A.C. Ferreira, Â. Silva, S. Teixeira, Multi-objective optimization of solar thermal systems applied to residential building in Portugal, in: T.E. Misra, O. Gervasi, B. Murgante, E. Stankova, V. Korkhov, C. Torre, A.M. Rocha, D. Taniar, B. Apduhan (Eds.), 19th Int. Conf. Comput. Sci. Its Appl. (ICCSA 2019), Lecture Notes in Computer Science, Springer, Saint Petersburg, 2019, pp. 26–39, https://doi.org/10.1007/978-3-030-24311-1_2.
[96] R. Beltran, N. Velazquez, A.C. Espericueta, D. Sauceda, G. Perez, Mathematical model for the study and design of a solar dish collector with cavity receiver for its application in Stirling engines, J. Mech. Sci. Technol. 26 (2012) 3311–3321, https://doi.org/10.1007/s12206-012-0801-0.
[97] J. Silva, L. Fraga, M.E. Ferreira, S. Chapela, J. Porteiro, S.F.C.F. Teixeira, J. Teixeira, Combustion modelling of a 20 kW pellet boiler, in: Energy, ASME, 6B, 2018, https://doi.org/10.1115/IMECE2018-88063. V06BT08A036.
[98] L.G. Fraga, J. Silva, J.C.F. Teixeira, M.E.C. Ferreira, D.F. Soares, S.F. Teixeira, The effect of the heating and air flow rate on the mass loss of pine wood particles, in: ECOS 2018 - Proc. 31st Int. Conf. Effic. Cost, Optim. Simul. Environ. Impact Energy Syst, Universidade do Minho. Departamento de Engenharia Mecânica, Guimarães, Portugal, 2018.
[99] A. Williams, J.M. Jones, L. Ma, M. Pourkashanian, Pollutants from the combustion of solid biomass fuels, Prog. Energy Combust. Sci. 38 (2012) 113–137, https://doi.org/10.1016/j.pecs.2011.10.001.
[100] J. Porteiro, J. Collazo, D. Patiño, E. Granada, J.C. Moran Gonzalez, J.L. Míguez, Numerical modeling of a biomass pellet domestic boiler, Energy Fuels 23 (2009) 1067–1075, https://doi.org/10.1021/ef8008458.
[101] D. Neves, H. Thunman, A. Matos, L. Tarelho, A. Gómez-Barea, Characterization and prediction of biomass pyrolysis products, Prog. Energy Combust. Sci. 37 (2011) 611–630, https://doi.org/10.1016/j.pecs.2011.01.001.
[102] P. Ribeiro, C. Vilarinho, M. Ferreira, E. Seabra, L. Fraga, J. Teixeira, Strategies for the design of domestic pellet boilers, in: Germano Veiga, José Machado, Filomena Soares (Eds.), Nnovation, Eng. Entrep. HELIX 2018. Lect. Notes Electr. Eng., Springer, Guimarães, Portugal, 2019, pp. 668–674, https://doi.org/10.1007/978-3-319-91334-6_91.
[103] B. Peters, Validation of a numerical approach to model pyrolysis of biomass and assessment of kinetic data, Fuel 90 (2011) 2301–2314, https://doi.org/10.1016/j.fuel.2011.02.003.
[104] J. Zarinchang, A. Yarmahmoudi, Optimization of thermal components in a stirling engine, in: WSEAS Trans. Heat Mass Transf, 2009, pp. 1–10.
[105] E. Cardozo, C. Erlich, A. Malmquist, L. Alejo, Integration of a wood pellet burner and a Stirling engine to produce residential heat and power, Appl. Therm. Eng. 73 (2014) 671–680, https://doi.org/10.1016/j.applthermaleng.2014.08.024.
[106] J. Huang, J. Fan, S. Furbo, D. Chen, Y. Dai, W. Kong, Economic analysis and optimization of combined solar district heating technologies and systems, Energy 186 (2019) 115886, https://doi.org/10.1016/j.energy.2019.115886.
[107] K. Wang, Y. Zhang, G. Sekelj, P.K. Hopke, Economic analysis of a field monitored residential wood pellet boiler heating system in New York State, Renew. Energy 133 (2019) 500–511, https://doi.org/10.1016/j.renene.2018.10.026.